ASSESSMENT OF CLIMATE VARIABILITY
OF THE GREENLAND ICE SHEET:
INTEGRATION OF IN SITU AND SATELLITE DATA

K. Steffen, W. Abdalati, J. Stroeve, A. Nolin, J. Box , J. Key, J.Zwally[1], M. Stober[2], J. Kreuter[2]
University of Colorado at Boulder
Cooperative Institute for Research in Environmental Sciences
Division of Cryospheric and Polar Processes
Campus Box 216, Boulder CO 80309

[1] Goddard Space Flight Center, Greenbelt, MD
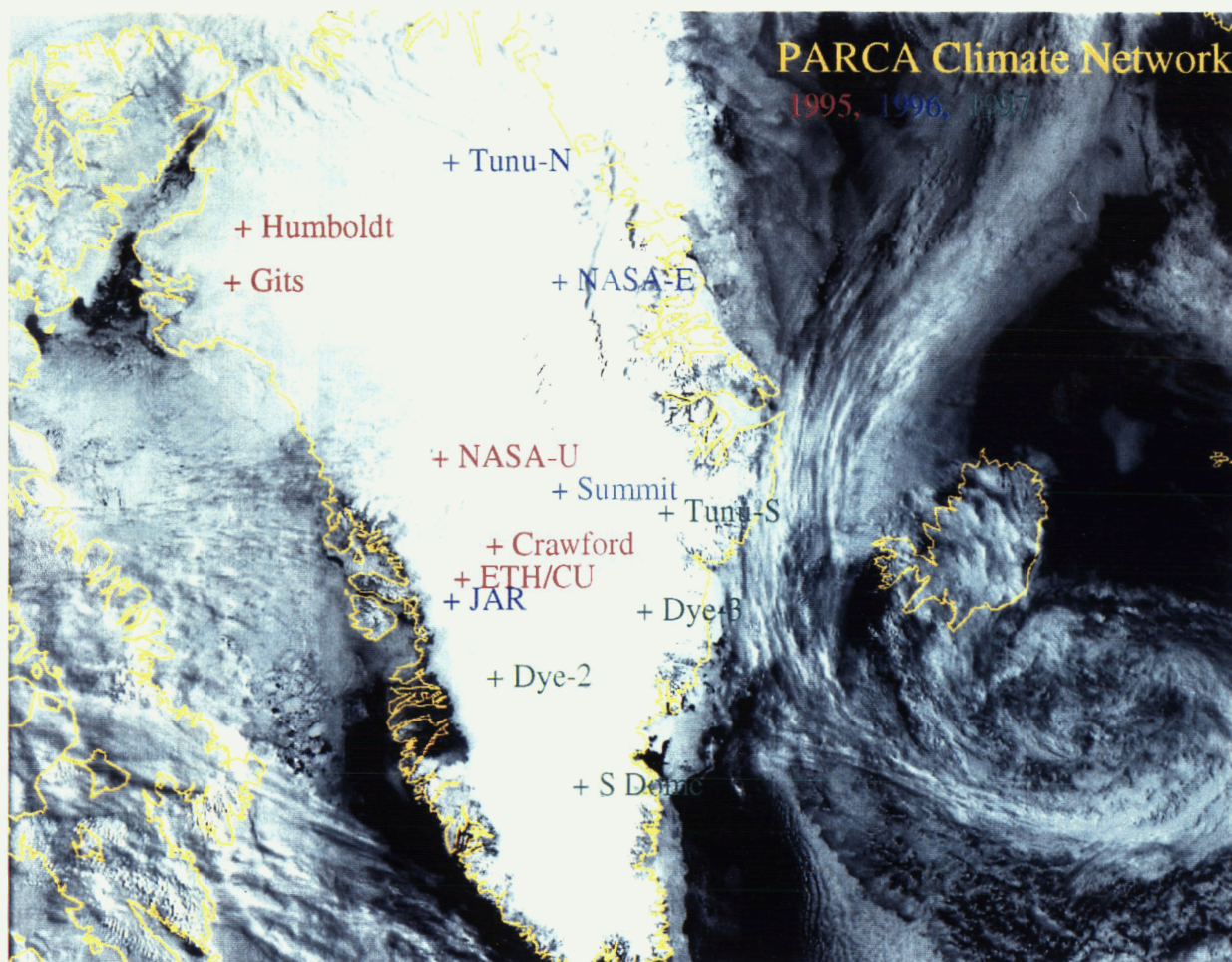[2] Fachhochschule Stuttgart, Germany

NAGW-2158
Progress Report
to
National Aeronautics and Space Administration

April 1996

TABLE OF CONTENTS

SUMMARY OF HIGHLIGHTS

AVHRR TIME SERIES AND SURFACE BASED RADIATION MEASUREMENTS

- The mean optical depth at the ETH/CU camp in spring is 7.8 ±2.1.

- The aerosol optical depth ranged from 0.05 to 0.09 for a typical spring day at the ETH/CU camp.

- Regression statistics of R^2 = 0.985, RMS (broadband estimate) = 0.657 were derived from pyranometer broad- and spectrometer narrowband reflectances for snow surfaces.

- A mean difference of 0.3 % albedo was found for AVHRR derived and surface based broadband albedo, neglecting the anisotropic nature of snow reflectance, for spring and summer months in 1990, 1991 and 1993.

- Larger differences between the AVHRR and observed surface albedo are found in August, with an underestimation of the surface albedo by 10% or more.

- The coldest areas on the Greenland ice sheet as identified from AVHRR thermal infrared measurements are identified with the high-elevation region (summit), but the coldest temperatures are not always located at the peak elevation. The location of minimum temperature can be found to move several hundred kilometers from month to month. In particular, during polar night the location of the minimum surface temperature is found to move further north, to latitudes as high as 76° N.

- During the polar night, the coldest surface temperatures as measured from AVHRR are found to occur in either December, January, or February. The greater variability in the winter surface temperatures reflects the variability in storms. During calm periods, extreme radiative cooling of the snow surface results in deepening the surface inversion.

- The interannual variability of average monthly summer temperatures is small, although 1992 was slightly colder than the other years, with the minimum temperature for all summer months (May-September) remaining below 250 K, which could be explained by the increase of the aerosol optical depth as a result of the Mount Pinatubo eruption.

- For AVHRR cloud detection over Greenland, the ice sheet must be divided into regions of dry snow and melting snow. Using this method, clouds were detected 87% of the time at the ETH/CU camp during summers 1990, 1991 and 1993.

PASSIVE MICROWAVE TIME SERIES

- Melt on the ice sheet as derived from passive microwave satellite data is found to be most extensive on the western side, and peaks in late July. An increasing trend is found in melt area between the years 1979-1991 of 4.5% per year, which came to an abrupt halt in 1992 after the eruption of Mt. Pinatubo.

- A similar increasing trend is observed in the temperatures at six coastal stations. The relationship between the warming trend and increasing melt trend between 1979 and 1991 suggests that a 1° C temperature rise corresponds to in increase in melt area of 85,000 km^2, which generally exceeds one standard deviation of the natural melt area variability.

- The sensitivity of passive microwave emissivity to accumulation is greater with increasing hoar layer thickness. This is most likely because the high scattering characteristics and large optical thickness of the hoar layer result in significant extinction of the upwelling radiation from the snow below.

- Emissivity is largely dependent on the hoar layer thickness itself. Variations in hoar thickness of a few millimeters, have roughly the same impact on the emissivity as ten centimeters of accumulation changes.

- The average date of minimum temperature for the SMMR - SSM/I coverage period (1978-1994) is January 17, with a standard deviation of 31 days. This variability is significant and should be accounted for.

- The radiative transfer model appears to accurately represent the emission behavior of snow under changing conditions of accumulation and hoar development. The link between microwave emission and accumulation rates in the dry snow area of the Greenland ice sheet is significant.

GEODETIC RESULTS FROM THE ETH/CU CAMP

- The actual ice flow velocity at the ETH/CU camp is 0,327 m day^{-1}. The azimuth of flow direction from the period 1994 to 1995 is $\alpha = 260.0790$ gon (average of 4 points in the deformation net). This value is only slightly different from the long periodic value from 1991 to 1994 ($\alpha = 260.6020$ gon).

- A surface height diminution of -0.375 m y^{-1} was found for the time period 1991 to 1994 at the ETH/CU camp, based on several GPS measurements. For the period 1991 to 1994 an ice surface height diminution of -0.20 m y^{-1} was found.

1. INTRODUCTION

1.1 Rational of the Study

The proposed research involves the application of multispectral satellite data in combination with ground truth measurements to monitor surface properties of the Greenland Ice Sheet which are essential for describing the energy and mass of the ice sheet. Several key components of the energy balance are parameterized using satellite data and *in situ* measurements. The analysis has been done for a 6 to 17 year time period in order analyze on the seasonal and interannual variations of the surface processes and the climatology.

Our goal was to investigate to what accuracy and over what geographic areas large scale snow properties and radiative fluxes can be derived based upon a combination of available remote sensing and meteorological data sets. Operational satellite sensors were calibrated based on ground measurements and atmospheric modeling prior to large scale analysis to ensure the quality of the satellite data. Further, several satellite sensors of different spatial and spectral resolution were intercompared to access the parameter accuracy. For the understanding of the surface processes a field program was designed to collect information on spectral albedo, specular reflectance, soot content, grain size and the physical properties of different snow types. Further, the radiative and turbulent fluxes at the ice/snow surface were monitored for the parameterization and interpretation of the satellite data.

The results include several baseline data sets of albedo, surface temperature, radiative fluxes, and different snow types of the entire Greenland Ice Sheet. These climatological data sets are of potential use for climate sensitivity studies in the context of future climate change.

1.2 Logistic Summary

We arrived at the ETH/CU camp on May 10, 1995. The station was occupied until June 19, 1995. The following members took part in the 1994 field expedition:

Name	Institution	Arr.	Dep.
Konrad Steffen	CU-Boulder	5-10	5-27
Jay Zwally	GSFC-NASA	5-10	5-19
Waleed Abdalati	CU-Boulder	5-10	6-19
Jason Box	CU-Boulder	5-10	5-19
Ken Jezek	BPRC-Ohio State	5-10	5-19
Ingrid Zabel	BPRC-Ohio State	5-10	5-19
Jeff Key	CU-Boulder	5-27	6-19
Jürgen Kreutter	FHS Stuttgart	5-27	6-19

We retrieved climatological and glaciological data recorded in our absence for 331 days. All sensors worked for the entire time period and there was no data loss.

2. SURFACE CLIMATOLOGY

2.1 Climate Monitoring at the ETH/CU camp

The climate recordings from the ETH/CU camp on the western slope of the Greenland ice sheet are probably the longest and most complete climate record for the entire ice sheet. A total of 20 climate variables were recorded at a temporal resolution of 3 hours continuously from 1991 through the present. The air temperature and wind speed at 10 m are shown in Fig. 2.1 for 1991-95. The data shown was processed with a 24-h averaging filter to reduce the short-term fluctuations. The air temperature has a maximum seasonal amplitude of 40° C, with mean values varying from 22° - 31° C for the time period discussed. This large interannnual variation of the temperature amplitude can be explained by a varying occurrence frequency of katabatic storms, which are responsible for the sudden temperature rise of up to 35° C in the middle of winter (see Fig. 2.1). The katabatic storms transport warmer air through turbulent mixing from the inversion height to the surface. Is has been shown in previous progress reports, that surface wind speed and temperature and are highly correlated, with the later having a time lag of 8 to 10 hours. The seasonal wind speed maximum coincide with the temperate minimum in the February-March time period.
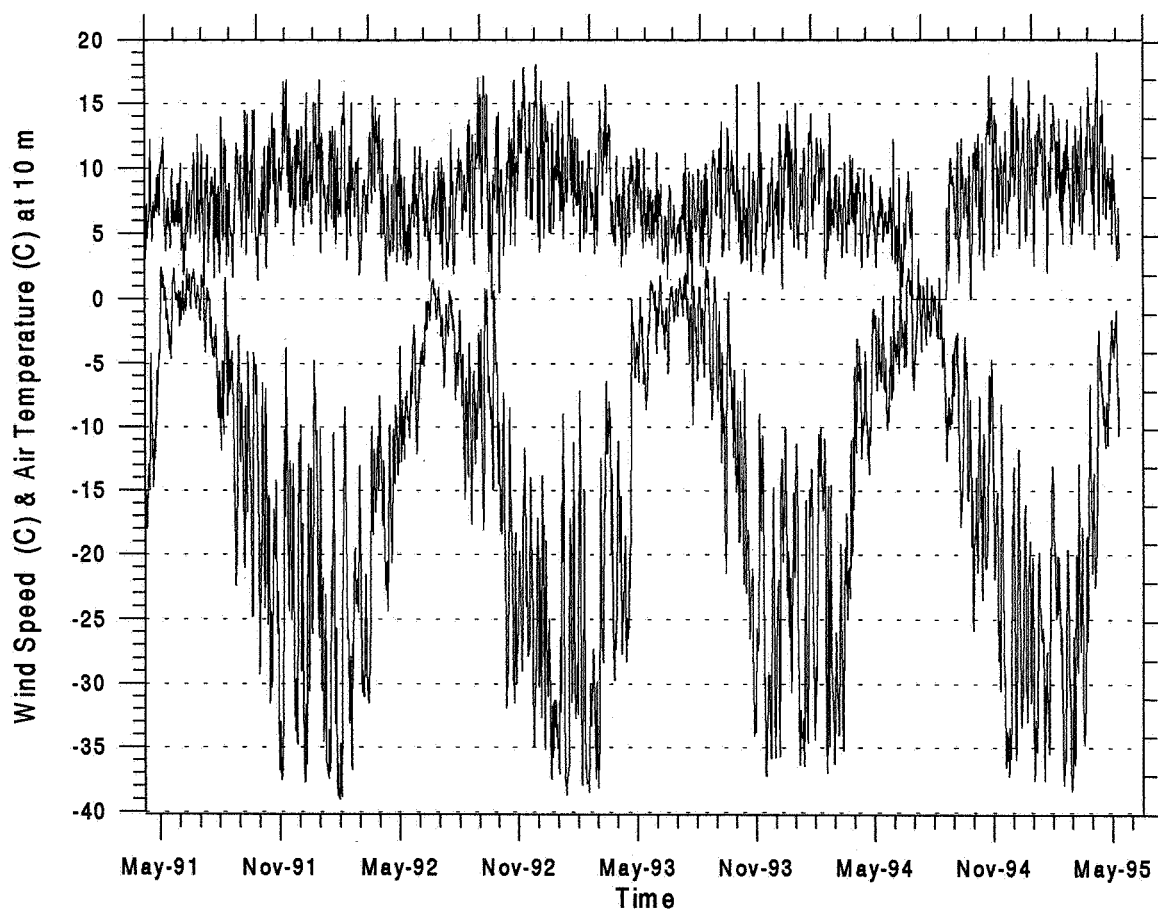

Figure 2.1   Surface temperature (lower curve) and wind speed (upper curve) records at 10 m above the snow surface for 1991 through 1995 at the ETH/CU camp near Jakobshavn.

2.2 Snow Accumulation along West Greenland

The first seven months of snow height recordings at the four automatic weather stations (AWS) reveal quite a variability in snow accumulation along the western slope of the Greenland ice sheet (Fig. 2.2). The two stations Crawford and NASA-U situated between 70-74° N, show a similar accumulation rate during the cold month October through December. It is interesting to note that the two sites have such a similar accumulation rate, given the fact that the are roughly 450 km apart, with NASA-U being at an elevation of 2400 m, compared to the Crawford site at 2000 m . Some snow surface lowering of 0.16 m occurred in July at the Crawford site, which can be attributed to snow compacting, snow sublimation, and possibly some melt. Accumulation rates for the two northern sites are markedly different, even though they are only 100 km apart. GITS along the western slope of the ice sheet has a high accumulation rate due to the up-slope effect of the Baffin Bay cyclone which dominates that regions. This area is also known to have the highest annual accumulation for northern Greenland, exceeding 60 cm water equivalent on an annual basis according to Ohmura and Reeh [1991]. The Baffin Bay moisture flux does not reach the Humboldt site in the northwest, as the cyclone path usually does not go that far north, and consequently, the Humboldt site has a much reduced accumulation rate. Recent ice core analysis from the Humboldt site revealed a mean annual accumulation of roughly 17 cm water equivalent over the past 60 years (R. Bales, personal communication).
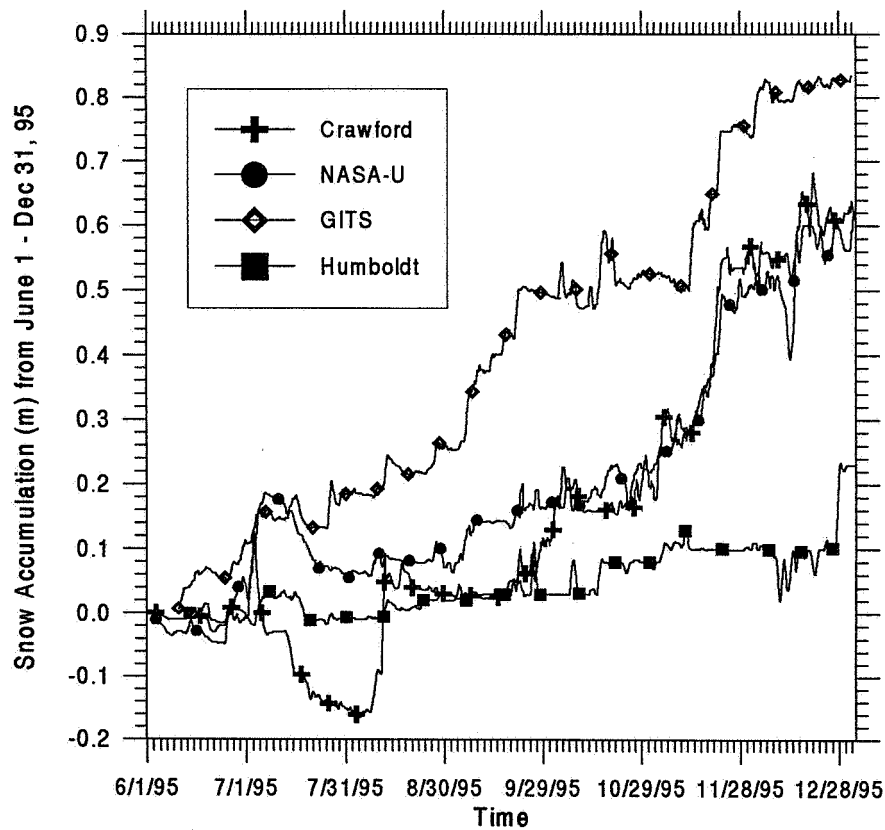

Figure 2.2   *Surface snow accumulation at four automatic weather stations along the western and northwestern slope of the Greenland ice sheet.*

2.3 Cloud Optical Depth

From the perspective of the surface radiation balance, cloud optical depth is a more robust quantity than the more commonly reported cloud fraction. Cloud optical depth is a measure of the cumulative depletion of radiation as it passes through a cloud. It therefore summarizes the scattering, absorption and extinction characteristics of clouds.

In theory this quantity can be estimated from downwelling short-wave radiation measurements at the surface by comparing the observed flux to a modeled flux. In practice this procedure requires knowledge of the temperature, humidity, aerosol, and ozone characteristics of the atmosphere since these parameters are also responsible for the depletion of solar radiation. If they are known then estimating the cloud optical depth is a simple matter of modeling the downwelling short-wave radiation in an iterative manner varying the cloud optical depth until the computed flux matches (or is within a few W m^{-2} of) the observed flux.

This procedure was applied to the Greenland surface radiation data using the Streamer radiative transfer model (Key, 1995). Values for unmeasured atmospheric characteristics (e.g., ozone) were estimated by finding values such that the computed clear sky flux matched the observed clear sky flux at a variety of solar zenith angles. An extensive look-up table was then generated over a range of surface albedos and cloud optical depths. Clouds in the liquid phase are assumed since we have no way of actually determining particle phase. This assumption is valid for much of the field season.

Results are shown in Figure 2.3. The mean optical depth is 7.8 (unit-less) with a standard deviation of 2.1. These values are consistent with other measurements of Arctic stratus cloud. It is important to note, however, that this is an "effective optical depth" since in many cases the cloud fraction is significantly less than unity; i.e., the procedure assumes that there is a uniform cloud cover, which is often not the case. Nevertheless, the cloud optical depth gives us important information about the effect of clouds on the surface radiation balance.
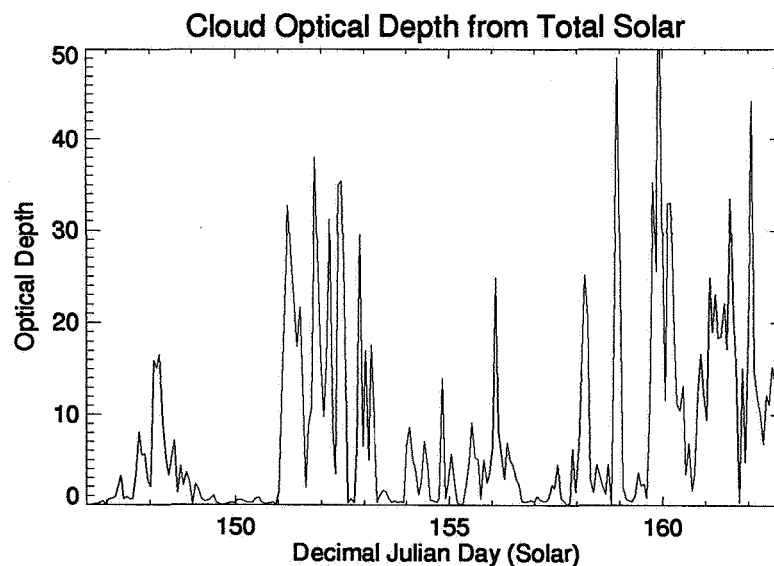

Figure 2.3   Cloud optical depth values derived from sunphotometer recordings at the ETH/CU camp in spring 1995.

3. SURFACE FLUXES FROM AVHRR

Monitoring and modeling the radiative surface fluxes over the time and space scales relevant for climate modeling and weather forecasting is not yet possible, due to the complexity of the physical system involved. Nor is it yet possible to estimate surface fluxes to within 5 W m^{-2}, the accuracy required for climate studies (Key et al., 1994), using satellite data. Satellite remote sensing techniques can however, provide some surface and atmospheric parameters that are useful for monitoring the surface fluxes over various time scales.

The observation of surface fluxes from satellite is complicated by the intervening atmosphere which scatters, absorbs and emits radiation. Therefore, atmospheric corrections are necessary to isolate those features of the observation which are intrinsic to the surface, from those caused by the atmosphere. Only after accurate atmospheric correction can one proceed to study seasonal and annual surface changes and to attempt the extraction of surface albedos and temperatures. The retrieval of surface albedo and surface temperature from AVHRR visible and thermal infrared data is discussed in the next section.

3.1 Shortwave Fluxes

3.1.1 Surface Albedo

To obtain the net short-wave fluxes at the surface, the surface albedo must be determined. The surface albedo can be determined from AVHRR channel 1 and 2 radiance's providing the following are taken into consideration: (1) atmospheric affects, (2) anisotropic nature of snow reflectance and (3) conversion from narrow to broadband albedo.

Previous studies showed some success in computing the surface albedo from AVHRR data in polar regions (De Abreu et al., 1994; Haefliger et al., 1993). However, these studies either assumed that snow reflection was isotropic and didn't convert from narrow- to a broadband albedo (Haefliger et al., 1993) or used correction schemes based on measured radiance's at the top of the atmosphere (De Abreu et al., 1994). It is well known that snow does not reflect solar radiation isotropically. Failure to account for the directional reflectance of snow can lead to errors as large as 50% in the total outgoing flux (Steffen,1987; Steffen, 1996).

3.1.2 Atmospheric Correction

Although the atmosphere is relatively thin in the polar regions, there is still significant attenuation of the surface radiation. A comparison between surface and coincidental TOA broadband albedos reveal that on average, 20% of the reflected radiation at the surface is attenuated before reaching the satellite during the summer months, and this attenuation varies seasonally. Less radiation is attenuated during the early summer months when the atmosphere is still relatively thin (May - June, ~17 %), and more during the later summer months (July and August,~23%).

Atmospheric correction of the AVHRR satellite radiance's can be accomplished by using the 6S radiative transfer model (Tanre et al., 1992). Using the 6S radiative transfer model, the effect of uncertainties in the input parameters on the satellite measured radiance's was studied. Uncertainties in aerosol amounts have the greatest impact on the satellite measured visible and near infrared radiance's, with errors of up to 3.3% for the visible channel with an aerosol uncertainty of 50%. This large value for the uncertainty in aerosol amount could be exceeded if stratospheric aerosol amounts were to increase for example during a volcanic eruption. It is important to note that at higher elevations the sensitivity is less. For example, at the ETH/CU camp elevation (1.155 km), the change in satellite reflectance for a 50% change in atmospheric visibility is only 1.1%.

Ozone is the next most important atmospheric constituent to consider when estimating AVHRR satellite radiance's in the visible channel. A 50% change in ozone concentration can lead to errors up to 1.5%. Uncertainties in atmospheric water vapor have the least impact on the visible and near infrared satellite radiance's.

Since aerosols have the largest impact on the satellite visible radiance's, measurements were made at the ETH/CU camp to determine the aerosol optical depth over the ice sheet. Results indicate that the atmosphere over the ice sheet is optically thin. The aerosol optical depth is determined from sun photometer measurements by subtracting from the total optical depth the contributions due to other atmospheric constituents, such as Rayleigh (molecular) scattering ($t_{rav}(l)$) and absorption by atmospheric gases such as ozone, water vapor, carbon dioxide, etc. ($t_{abs}(l)$). Figure 3.1 shows the diurnal variation of the aerosol optical depth on May 24, 1995. Values of the aerosol optical depth range from 0.05 to 0.12 in the Arctic (Binenko and Harshvardhan, 1993). Thus, the values found at the ETH/CU camp of 0.05-0.09 are at the lower end for values found in the Arctic.
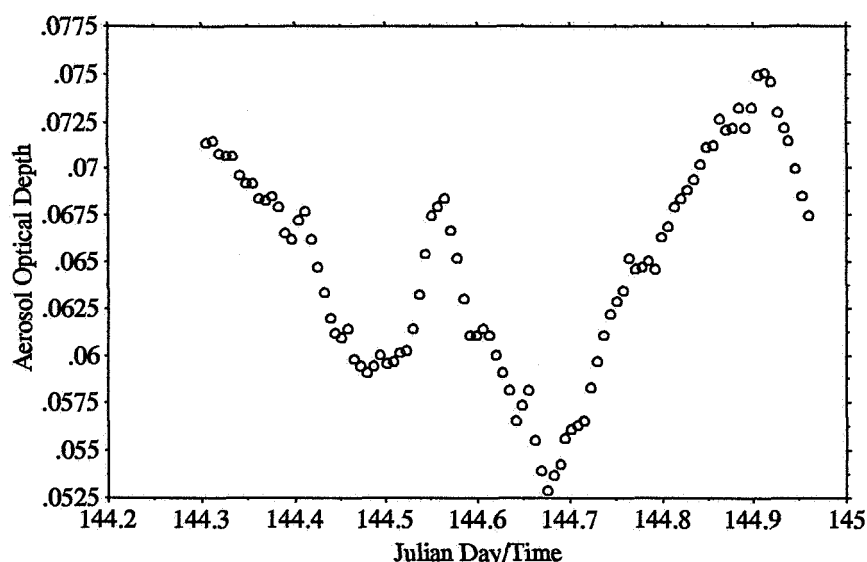

Figure 3.1   Diurnal variation of aerosol optical depth at 0.55μm measured at the ETH/CU camp on May 24, 1995.

The atmospheric inputs used in the 6S model include the following: (1) continental aerosol model with a "visibility" of 50 km (optical depth at 0.55 μm of 0.152 at sea level elevation) and (2) arctic summer profile (water vapor is based on radiosonde launches from the ETH/CU camp: 1.02 g cm^{-2} column water vapor; 0.331 cm-atm total ozone at sea level elevation).

3.1.3 Broadband Albedo Parameterization

Since the AVHRR multispectral narrowband radiometric scanners only measure the reflectance in a few narrowband channels they need proper adjustments so that these data can be used to estimate broadband albedo values. To estimate the surface broadband albedo, previously determined relationships between planetary narrow- and broadband albedo, such as those of Wydick et al. (1987) and Li and Leighton (1992), cannot be used. This is because, the spectral behavior is very different at the surface and top of the atmosphere due to the relative fraction of direct and scattered solar beams, varying with atmospheric turbidity and the snow spectral reflectivity. Therefore, the atmosphere attenuates the radiance differently in the visible and near infrared AVHRR channels and a new relationship is necessary.

As for the conversion from narrowband satellite to planetary albedo, a linear relationship is sought, relating the surface broadband albedo to the atmospherically corrected AVHRR channel 1 and 2 reflectances. This new expression is based on surface measured narrow- and broadband albedo data collected from the ETH/CU expedition camp. Daily hemispheric-spectral albedo measurements made with the portable spectrometer serve as the narrowband visible and near infrared data set. Coincident solar measurements with the set of Eppley Pyranometers provide the surface broadband albedo. Since two different instruments are used, the relative accuracy of the albedo values is estimated to be approximately 0.7% (Haefliger et al., 1993).

Table 3.1 shows the regression results of using both channels as predictors of the surface broadband albedo, and Figure 3.2 compares the resulting model predicted with observed broadband albedo. Using both channels increases the accuracy of the broadband albedo estimate (accuracy of 0.657) and explains approximately 98.5% of the variance associated with surface broadband albedo.

Table 3.1   Regression statistics derived from Pyranometer broad- and Spectrometer narrowband reflectances for snow surfaces. $R^2 = 0.985$, RMS of broadband estimate = 0.657

Variable	Coefficient	Standard Deviation	Probability
Constant (a) (%)	4.123		
Channel 1 (b_1)	0.655	0.055	0.0001
Channel 2 (b_2)	0.216	0.037	0.0001

This new relationship will give the surface broadband albedo from atmospherically corrected AVHRR VIS and NrIR reflectances. If Li and Leighton's TOA broadband relationship is used instead, the estimated surface broadband albedo is on average 5% lower than the observed broadband albedo. Note however, before the above equation can be applied, it is necessary to correct for the anisotropic nature of snow reflectance.

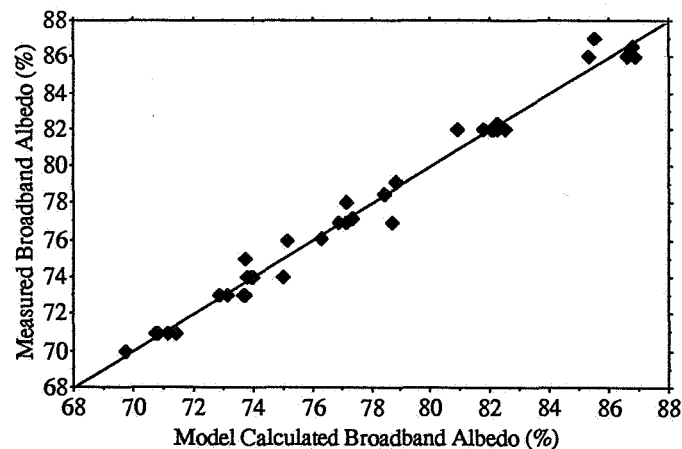*Figure 3.2.   Comparison of albedo predicted using the surface based model with pyranometer albedo observations from the ETH/CU camp. Data are from 1990, 1991 and 1993.*

3.1.4 Accuracy of the Surface Albedo

Figure 3.3 shows the AVHRR and observed surface broadband albedo for clear sky only during summer 1990 (June - August) at the ETH/CU camp. Anisotropic reflectance factors (ARFs) were modeled

by Anne Nolin   and were used to correct the AVHRR surface albedos (e.g. albedo_true = AVHRR_albedo/ARF). For all months, neglecting the anisotropic nature of snow reflectance, results in mean difference between the observed and calculated surface albedo of 0.314% albedo, standard deviation of 4.53%. Including the anisotropic effects of snow reflectance has a mean difference of 4.56% albedo, standard deviation of 4.86%. However, if we just look at the month of June, the differences become -3.29% (std. dev. 1.18%) and 1.35% (std. dev.=1.36%) ,with and without ARF, respectively.

Larger differences between the AVHRR and observed surface albedo are found in August, with an underestimation of the surface albedo by 10% or more. During August, the reflectances measured by the visible and near infrared channels are about 10% less than during June. Therefore, it would seem that more of the reflected radiation at the surface is being attenuated before reaching the satellite sensor. An examination of atmospheric water vapor calculated from radiosonde launches made at the ETH/CU camp reveal no significant difference in column water vapor amounts for June and August. Therefore, it is unlikely that the error is caused by inaccurate values of the column water vapor. Perhaps, the error is caused by an increase in atmospheric aerosols. Uncertainties in aerosols do have the largest impact on the visible radiances, although maximum aerosol concentrations over the Greenland ice sheet tend to occur during spring (Jaffrezo et al., 1993; Jaffrezo and Davidson, 1992; Hillamo et al., 1993).

However, even if an aerosol concentration uncertainty of 50% was used in the 6S model, the discrepancies found could not be explained. A source of error could also be the values of the anisotropic reflectance factor (ARF). These values are based on modeled values of the bi-directional reflectance distribution function for snow, which were tabulated for 6 viewing zenith angles (0, 15, 30, 45, 60 and 75°), 10 relative azimuth angles (0 - 180° in 20° increments), and 6 solar zenith angle for AVHRR channel 1 (0, 15, 30, 45, 60, 75 and 85°) and 18 solar zenith angles for AVHRR channel 2 (0 - 85° in 5° increments).

Other errors could be due to clouds that contaminated the AVHRR GAC pixel. The criteria used for flagging the camp pixel as cloudy was based on synoptic observations. Synoptic cloud observations during 1990 were available at 3 hour intervals only, and did not coincide exactly with the time of the satellite overpass. Further errors will result from comparing half hourly measurements of the surface albedo at a point, with an instantaneous satellite measurement spanning 4 km. In addition, calibration of AVHRR channel 1 and 2 was done using the NOAA/NASA Pathfinder time-dependent calibration coefficients and are likely to be off by a few percent (Rao and Chen, 1995). From the above, it seems that there are still significant difficulties in retrieving accurate snow surface albedo.
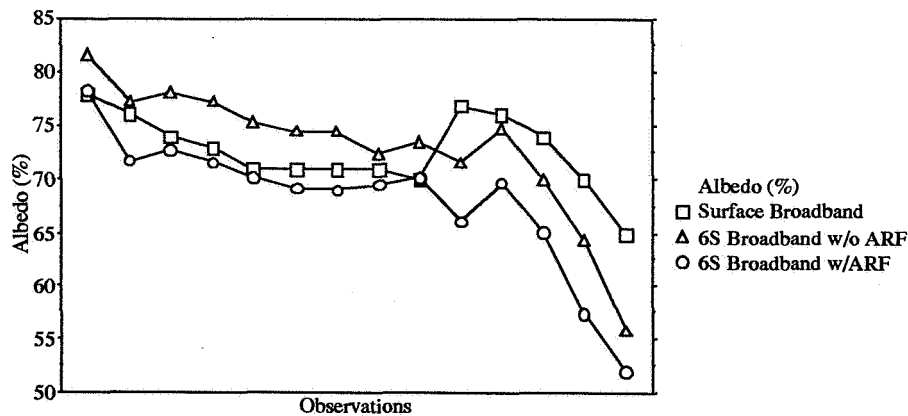

Figure 3.3.   Comparison between observed and AVHRR computed broadband albedo at the ETH/CU camp for clear sky only during 1990.   Shown is the AVHRR surface broadband albedo with and without correcting for the anisotropic nature of snow reflectance.

3.2 Longwave Fluxes

3.2.1 Surface Temperature

Computation of the upwelling surface longwave flux requires accurate knowledge of the surface temperature and emissivity.   To obtain surface temperatures from satellite thermal radiances requires the removal of the effects of the Earth's atmosphere.   Although the surface emitted energy in the infrared window channels is attenuated very little as it passes through the cloud-free polar atmosphere, it can be as large as 3 K during summer (Fig. 3.4). In addition, the correction from satellite brightness temperature to surface temperature can be of either sign (i.e. sometimes the surface temperature is greater than the satellite measured temperature, sometimes the reverse is true). During winter the correction is expected to be smaller due to the extremely low moisture content of the winter Arctic atmosphere (column water vapor ~0.2 g cm^{-2} during Arctic winter, from ISCCP C2 data set).

Unfortunately, temperature and water vapor profiles at the time and location of the measurement to be corrected generally are not available for the Greenland ice sheet, although profiles of atmospheric temperature and water vapor are available from a few coastal stations around the ice sheet and from the ETH/CU camp during summers 1990, 1991 and 1993. Because of the lack of *in situ* atmospheric profile data, the use of the radiative transfer method is limited, and another must be sought.
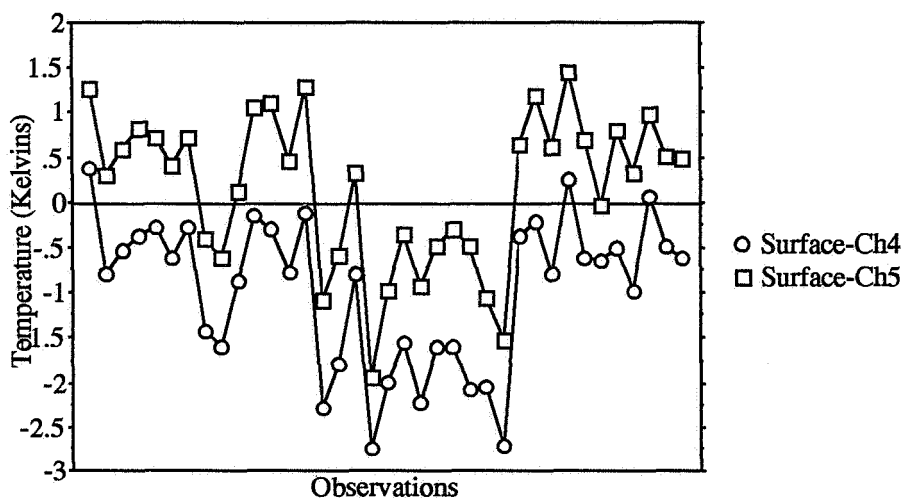

Figure 3.4   Surface temperature minus coincident AVHRR GAC satellite brightness temperature for the two thermal channels (T_4 and T_5) for clear skies, measured at the ETH/CU camp during summers 1990 and 1991.

Alternatives to using a radiative transfer model do exist, such as the "split-window" technique that uses two differentially absorbing thermal infrared channels between 10 and 13 μm (McMillin, 1975) and is currently used operationally by NOAA in deriving sea surface temperature (SST) (McClain et al., 1985). However, the determination of surface temperature using this method, is in general limited by the variability of the surface emissivity (e.g. Price, 1983). Dozier and Warren (1982) showed that the infrared emissivity of snow is primarily a function of viewing angle and not dependent upon snow properties. If this assumption is valid, then it is possible to extract snow surface temperatures using a similar methodology as for SST retrieval.

However, recent snow emissivity measurements by Salisbury et al., (1994) showed the emissivity to be dependent upon snow grain size and packing fraction, causing snow emissivity to be as low as 0.95 at 13 μm for coarse granular snow. This can result in temperature measurements at nadir to be in error by as

much as 3 K (Wald, 1994). With respects to the AVHRR thermal channels, using the emissivity values as given by Salisbury et al. (1994) instead of those of Dozier and Warren (1982) results in a 0.75 K temperature difference for channel 4, and 1.32 K for channel 5.

Fortunately, at the wavelengths of the AVHRR thermal channels, angular effects on emissivity have been found to be much greater than those due to snow grain size or packing effects for naturally occurring snow (Wald, 1994). Failure to account for the effect of viewing angle can lead to temperature errors as large as 1.5 K for the AVHRR viewing angles.

The "split-window" approach has been employed in polar regions using AVHRR data (Haefliger et al., 1993; Key and Haefliger, 1992, Lindsay and Rothrock, 1994) with some success. The regression model applied in these studies is of the form:

$$T_S = a + bT_4 + cT_5 + d((T_4\text{-}T_5)\sec(q))$$

where T_S is the surface temperature, T_4 and T_5 are the satellite brightness temperatures for AVHRR channels 4 and 5 respectively, q is the satellite viewing angle, and the coefficients a, b, c, and d were determined through a least squares regression between modeled AVHRR brightness temperatures and surface temperature.

Using local rawinsonde data, AVHRR derived surface temperatures in the Arctic using the above formulation have been given with an accuracy of 0.1 K (Key and Haefliger, 1992). Similarly, for the Greenland ice sheet, radiosonde data and measured surface temperatures from the ETH/CU camp were used to derive surface temperatures with maximum differences of 0.6 K (Haefliger et al., 1993). These accuracies are based on the regression analysis only of the modeled data, and do not include measurement errors. To obtain these accuracies, however, required local data and seasonal variations in atmospheric conditions were found to be important. In addition, mixing coefficients and data from different NOAA satellites adds errors of up to 1.0 K.

Furthermore, the validity of the method depends on the accuracy with which the snow surface emissivity can be estimated, and on the atmospheric attenuation for the two channels remaining in proportion. The latter assumption can break down for atmospheres with very low water vapor concentrations since absorption by CO_2 will begin to dominate and is more absorbing at 11 µm than at 12 µm. The errors induced by changing atmospheric conditions can be remedied by the use of satellite thermal radiances measured at different viewing angles (Stroeve et al., in press). The above mentioned studies also relied on the modeling of the snow surface emissivity according to Dozier and Warren (1982), the accuracy of which has been disputed by Salisbury et al. (1994).

Although the algorithm of Haefliger et al. (1993) has some shortcomings, it will be used in this study. The algorithm was based on measurements made locally on the Greenland ice sheet and is therefore, viewed as the most accurate method currently available for use with AVHRR thermal infrared data. Without any other *in situ* surface temperature measurements, such as during polar winter or at different elevations, it is impossible to derive an alternative model. It is also impossible to include the effects of changing grain size on snow emissivity, as information on grain size is not available on a large scale. These limitations, along with errors due to undetected clouds, will be regarded as part of the data error which is assessed by comparisons with *in situ* data.

3.2.2 Accuracy of the Surface Temperature

Surface temperatures were derived for each clear sky pixel from AVHRR GAC data during 1990 and 1991 when coincident surface temperature measurements were available from the ETH/CU camp. Fig. 3.5 shows a comparison of the observed surface temperature and the satellite derived surface temperature.

Direct comparison shows good agreement at the lowest temperature as well as at mid and high values. At around 271 K and 260 K the largest differences occur. The mean difference between the "true" and calculated surface temperature is -0.189 K with a standard deviation of 0.902 K. The maximum difference in temperatures is 2.2 K. Some of the error in the calculated surface temperature is a result of clouds which went undetected and thus contaminated the camp pixel. As mentioned before, synoptic cloud observation only were available at 3 hour intervals, and therefore, do not coincide exactly with the time of the satellite overpass. Other errors are a result of comparison between measured surface temperature at half hour intervals with instantaneous satellite measurements. Additional errors are present as a result of the previously mentioned errors due to varying atmospheric conditions and emissivity. Regression analysis of this data yields the following result:

$$T_S(meas) = 30.241 + 0.888 \ T_S(calc)$$

with a correlation coefficient of 0.966 and RMS of 0.761 K. $T_S(meas)$ is the observed surface temperature and $T_S(calc)$ is the surface temperature from AVHRR. AVHRR surface temperature data can therefore, be made more compatible with *in situ* ice sheet data by using the above equation to normalize corresponding values on the ice sheet. However, it is not known how representative the *in situ* data used in the analysis are for the entire ice sheet. There might be local effects that need to be accounted for, such as elevation changes. It is difficult to assess these affects without other *in situ* surface temperature data. However, it is estimated that the average deviation of AVHRR surface temperatures from the "true" surface temperatures is less than 1 K, which is within the uncertainty of the measurement.
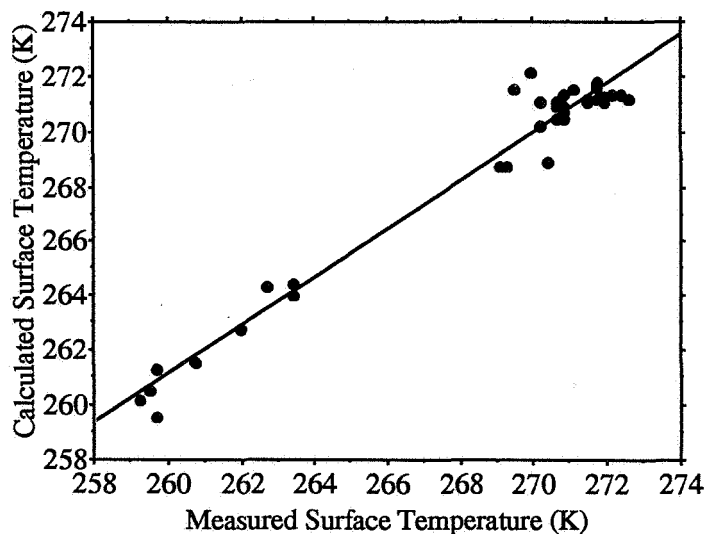
Figure 3.5   *Comparison between measured and calculated surface temperature during 1990 and 1991 at the ETH/CU camp. Data are for clear skies only. Regression of the data results in a line given by y = 30.241 + 0.888x, R^2=0.966, RMS=0.761K.*

3.2.3 Results

The degree of coolness of the ice sheet is dominated by its elevation. As the surface elevation increases, the temperature gradually decreases and minimum temperatures are found to occur at the summit region. The spatial characteristics of the ice sheet topography indicate that there is a strong coherence of temperature isotherms observed from AVHRR with the elevation contours. Figure 3.6 shows the surface

temperature versus elevation during June 1993 for a transect through the ETH/CU camp. The figure indicates there is a good correlation between the two variables, with a correlation coefficient of 0.81.

As shown in Table 3.2 the coldest areas are identified with the high-elevation region (summit), but the coldest temperatures are not always located at the peak elevation. The location of minimum temperature can be found to move several hundred kilometers from month to month. In particular, during polar night the location of the minimum surface temperature is found to move further north, to latitudes as high as 76° N.

Figure 3.7 gives the mean monthly surface temperatures at the ETH/CU camp, at the summit and average and minimum surface temperatures for the entire Greenland ice sheet from January 1989 through October 1993. Data is missing between January and May 1990. During the summer months, the warmest temperatures occur during the month of July, with the greatest temperatures found at the ETH/CU camp (~270 K). The ETH/CU camp is located at the equilibrium line altitude and tends to experience significant melt during the summer months. During melt, the surface albedo drops as low as 0.6, doubling the amount of solar energy absorbed by the snow pack and thereby increasing the snowpack temperature. At the summit, the snow does not melt and the summer surface temperatures remain well below 270 K. We also find that the minimum surface temperatures closely match those found at the summit during summer.

The interannual variability of average monthly summer temperatures is not great, although 1992 was slightly colder than the other years, with the minimum temperature for all summer months (May-September) remaining below 250 K. Summer 1992 is characterized by the almost lack of a melt period, with melt seemingly only occurring during the first two to three weeks in July only. Passive microwave observations (Abdalati pers. comm.) also suggest minimum melt extent for 1992. The cooler temperatures during summer 1992 could perhaps be explained by the eruption of Mount Pinatubo that loaded the stratosphere with a large amount of optically active aerosols (Minnis et al., 1993). Another event which probably influenced the Greenland climate was the El Nino event of 1992 which affected the global heat balance. During this period, 1992-1993, surface air temperatures were also found to be significantly colder over the entire Northern Hemisphere land areas (Greenland was excluded from the analysis), associated with an increase in the Northern Hemisphere snow extent (Groisman et al., 1994).

During polar night, the coldest surface temperatures are found to occur in either December, January, or February. The greater variability in the winter surface temperatures reflects the variability in storms. During calm periods, extreme cooling of the snow surface results and large surface inversions form. The typical scenario is that as the wind speed drops, the surface temperature begins to fall the surface inversion establishes itself. Temperatures then cool much more rapidly. When a storm occurs, temperatures at the snow surface rise as a result of mixing with the warmer maritime air (Miller, 1956). During such periods, surface temperatures may rise by as much as 20 degrees or more. The warm temperatures are usually accompanied by an increase in wind speed (katabatic winds), with the wind speed picking up sooner than the surface temperature.

Table 3.2   Greenland Summer Surface Temperatures (Minimum Temperature and Location, Average Temperature)

| Month	Year	Latitude (°N)	Longitude (°W)	T_{min}	T_{ave}
January	1989	74.3	35.4	220.6	234.7
February	1989	73.1	33.2	210.9	235.6
March	1989	76.2	41.3	223.7	239.8
April	1989	76.2	44.3	237.2	251.1
May	1989	70.2	37.7	247.8	255.4
June	1989	74.4	42.1	258.8	265.5
July	1989	71.9	37.6	258.2	266.3
August	1989	71.9	37.2	255.1	263.2
September	1989	72.5	37.7	236.8	252.3
October	1989	76.0	45.9	235.3	247.3
November	1989	76.0	38.3	227.8	243.1
December	1989	75.2	42.9	228.2	242.0
May	1990	74.5	39.9	247.9	263.0
June	1990	74.9	41.5	259.4	266.3
July	1990	70.7	43.0	253.6	266.8
August	1990	71.8	37.9	256.6	263.6
September	1990	72.4	39.9	248.2	254.8
October	1990	71.6	37.1	231.5	246.5
November	1990	75.6	39.1	228.6	242.1
December	1990	71.2	37.6	220.6	234.7
January	1991	70.0	37.5	217.9	234.0
February	1991	71.3	45.7	230.5	238.4
March	1991	74.6	38.4	229.7	244.8
April	1991	75.5	38.1	226.8	247.1
May	1991	74.0	42.0	230.2	246.6
June	1991	73.2	39.4	255.6	265.5
July	1991	76.4	43.7	256.8	266.5
August	1991	70.1	39.0	248.1	261.6
September	1991	72.5	36.6	238.6	255.1
October	1991	76.0	45.4	230.5	246.3
November	1991	73.1	39.5	217.3	237.7
December	1991	71.7	37.6	221.2	238.0
January	1992	72.0	38.7	220.7	237.4
February	1992	73.9	38.6	219.4	233.2
March	1992	75.0	39.2	223.5	239.2
April	1992	75.1	42.7	234.9	247.4
May	1992	69.8	42.9	245.7	254.3
June	1992	71.4	38.5	248.2	262.0
July	1992	72.2	31.0	251.8	264.9
August	1992	72.3	39.9	251.2	261.7
September	1992	72.5	37.0	241.2	254.2
October	1992	72.9	38.1	220.3	249.0
November	1992	75.8	38.7	215.8	238.8
December	1992	71.8	39.3	219.8	233.9
January	1993	74.5	38.5	215.0	229.9
March	1993	76.3	43.8	224.7	238.4
April	1993	72.4	36.9	239.0	249.1
May	1993	69.5	43.1	247.0	257.9
June	1993	72.9	38.6	259.2	265.0
July	1993	73.4	34.0	258.5	266.8
August	1993	73.7	35.6	252.0	262.0
September	1993	71.4	37.8	247.3	255.4
October	1993	75.8	42.9	228.6	246.8
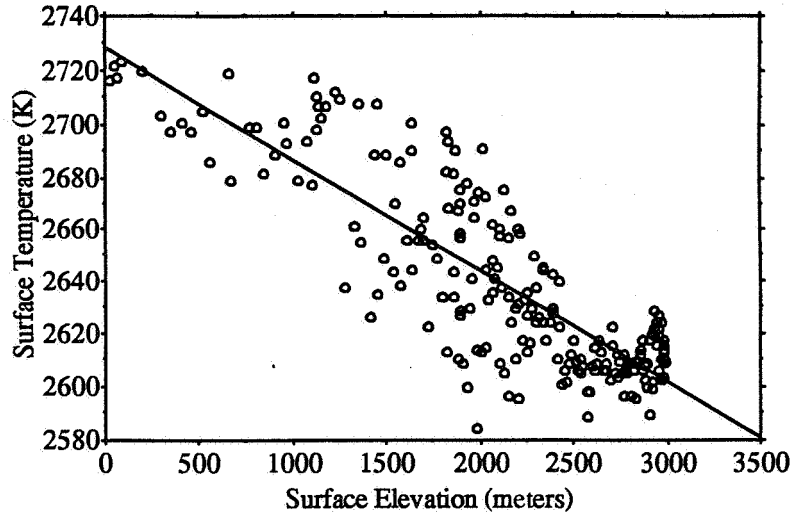
Figure 3.6   *Elevation versus AVHRR surface temperature over the Greenland ice sheet from a transect through the ETH/CU camp during June 1993.*
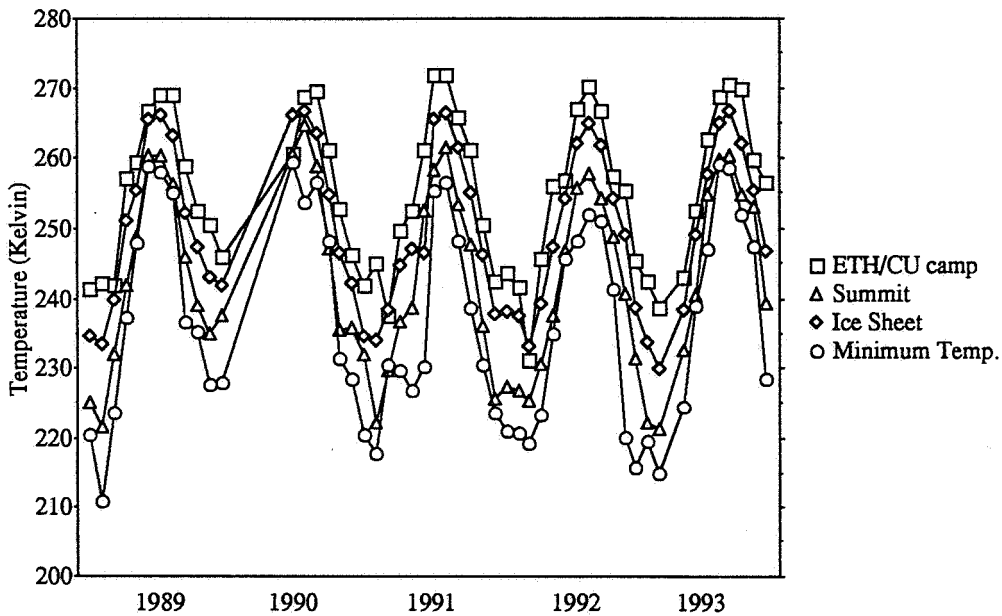

Figure 3.7   *Mean monthly surface temperatures at the ETH/CU camp and at the summit are shown with average and minimum surface temperatures for the entire Greenland ice sheet from January 1989 through October 1993. Data is missing between January and May 1990*

3.3 Cloud Detection

The main hindrance in retrieving accurate surface albedo and surface temperature from visible and thermal infrared satellite data is the inability to accurately detect clouds. Unfortunately, in polar regions, there still is not a reliable cloud masking method. This is because some cloud conditions exhibit the same spectral response as clear sky. For example, low, warm clouds during winter that are optically thick have similar temperatures as the underlying surface and often go undetected.

To define the threshold values that provide the most sensitive and reliable separation of cloudy and clear conditions is difficult. There are however, some significant spectral differences in the reflection and emission properties of water and ice which can help to identify clouds. For example, snow is highly reflective in the visible but quickly becomes absorptive towards the near-infrared (Warren and Wiscombe, 1980). Water clouds on the other hand are highly reflective throughout the solar spectrum till about 5μm (Saunders and Kriebel, 1988). For optically thick water clouds, the reflectance decreases only slightly in the NrIR and anisotropy effects are similar in AVHRR channel 1 and channel 2 and thus tend to cancel each other. Therefore, the ratio of the NrIR to the VIS reflectance is close to 1 (i.e. $a_2/a_1 \sim 1$), and these clouds show contrasts against the snow and ice underneath (even greater contrasts when the snow surface is melting). In the thermal infrared they might often be warmer than the surface underneath. Ice clouds on the other hand behave radiatively like snow layers in the visible, but are often colder than the polar snow underneath.

During daylight periods, low level water clouds show little contrast in the thermal infrared against the snow/ice surfaces but they appear considerably warmer at 3.7 μm since they reflect up to 30% of the incident solar radiation at this wavelength. This is true for cirrus clouds as well since they have higher transmissivities at 3.7 μm (Key and Barry, 1989). During the dark winter season, they tend to appear colder at 3.7 μm, but cirrus clouds will still appear warmer. High level ice clouds tend to have slightly lower emittance/absorptance at 10.5 μm than at 12.5 μm and thus might be warmer at 10.5 μm. However, for optically thick cirrus clouds, they tend to be colder at 10.5 μm than at 12.5 μm.

One means to detect clouds is the use of the difference between the radiances in AVHRR channel 4 and channel 5. There is a noticeable difference between the emission at 10 and 12 μm for clear and cloudy skies. However, the brightness temperature difference $DT = T_{10.8} - T_{12}$ is near zero for both clear skies and for overcast skies filled with optically thick clouds. Thus, optically thick clouds can not be detected using a threshold based on brightness temperature differences alone. Thin clouds however exhibit variable values of DT and can be detected as deviations of DT from zero. Optically thick clouds can however be detected using the ratio of channel 2 to channel 1 reflectance. Based on the above considerations, the following describes the cloud masking criteria during daylight.

Over Greenland, it was found important to separate the ice sheet into regions of dry snow and melting snow. For both regions however, the same process applies. Pixels are initially labeled as "clear" if:

(1) $|T_4 - T_5| < 0.7$ K,

(2) $r_3 < 3.0$ and

(3) $a_2/a_1 < 0.9$.

From these "clear" pixels, statistics are computed to test for erroneous values. Pixels are then labeled as "cloudy" if:

(1) $T_4 < mean(T_4(clear)) - std.dev(T_4(clear))$,

(2) $T_4 > mean(T_4(clear)) + std.dev(T_4(clear))$ and

(3) $r_3 > mean(r_3(clear)) + std.dev(r_3(clear))*4$.

Using this method, clouds were detected 87% of the time at the ETH/CU camp during summers 1990, 1991 and 1993.

The detection of clouds during polar winter is proving to be much more difficult due to the small contrasts in brightness temperature differences for clear and cloudy skies. During the polar night, large surface inversions occur causing differences in brightness temperatures on the order of those found for cloudy skies. Furthermore, after storms pass, it takes some time for the surface inversions to reestablish themselves, leading to varying degrees in the brightness temperature differences. Therefore, an automated algorithm using thresholds based brightness temperature differences between the two thermal channels is not reliable. The polar nighttime algorithm is therefore, still not complete.

4. PASSIVE MICROWAVE DERIVED MELT AREAS

4. 1 Introduction

The melt extent of the snowpack on the Greenland ice sheet is of considerable importance in terms of mass and energy balance on the ice sheet, as well as Arctic and global climates. Because wet snow absorbs significantly more incident solar radiation than dry snow, the ice sheet comprises an unstable, positive feedback component of the climate system. In addition, the large size and gentle slope of most of the Greenland ice sheet, causes small changes in the air temperature to create large areal changes in the dry and wet snow facies; thus underscoring the sensitivity of ice sheet melt to variations in climate. To better understand the ice sheet melt conditions and their relationship to the climate, seasonal and interannual variations in the areal melt extent are examined.

3.2 Method

By comparing passive microwave satellite data to field observations, variations in melt extent have been detected by establishing melt thresholds in the cross-polarized gradient ratio (XPGR). The XPGR, defined as the normalized difference between the 19 GHz horizontal channel and the 37 GHz vertical channel of the Special Sensing Microwave Imager (SSM/I), exploits the different effects of snowpack wetness on emission at different frequencies and polarization and establishes a distinct melt signal (Abdalati and Steffen, 1994). The thresholds for SSM/I instruments are shown in Figure 4.1. Using this XPGR melt signal, seasonal and interannual variations in melt extent of the ice sheet are studied for the years 1978 through 1994.

4.3 Results

Melt on the ice sheet is found to be most extensive on the western side (Fig. 4.2), and peaks in late July (Fig. 4.3). Moreover, there is a notable increasing trend in melt area between the years 1979-1991 of 4.5% per year (Fig. 4.4), which came to an abrupt halt in 1992 after the eruption of Mt. Pinatubo. A similar increasing trend is observed in the temperatures at six coastal stations. The relationship between the warming trend and increasing melt trend between 1979 and 1991 suggests that a 1° C temperature rise corresponds to in increase in melt area of 85,000 km^2, which generally exceeds one standard deviation of the natural melt area variability.

Analyses comparing Mote and Anderson's (1995) 37 GHz melt model results to those using the XPGR technique show good agreement in spatial melt extent. They also show that while the XPGR technique responds to deeper and more developed melt, the 37 GHz is more sensitive to surface melt. In the future, a combination of the two methods should yield a more complete description of the degree of melt development.
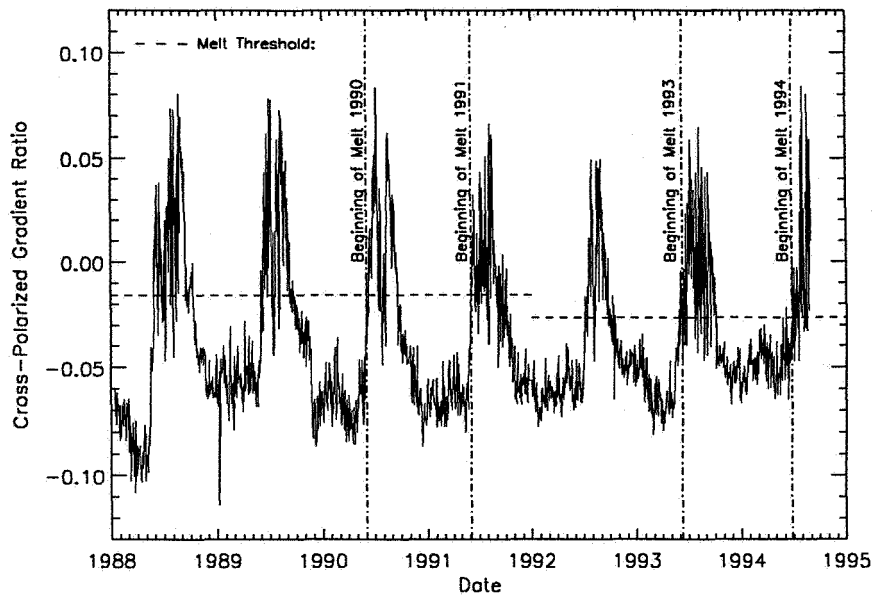
Figure 4.1   Cross-polarized gradient ratio (XPGR) time series for the ETH/CU camp pixel for the dates of available SSM/I data. Also shown are the dates on which melt was observed to begin at the camp, and the corresponding XPGR threshold associated with melt. There are two thresholds: XPGR = - 0.158 for the F8 SSM/I and XPGR = -0.0265 for the F11 SSM/I. The latter also applies to the SMMR instrument. Two thresholds are necessary in part because of instrument differences, but primarily because of the different crossover times of the two instruments.

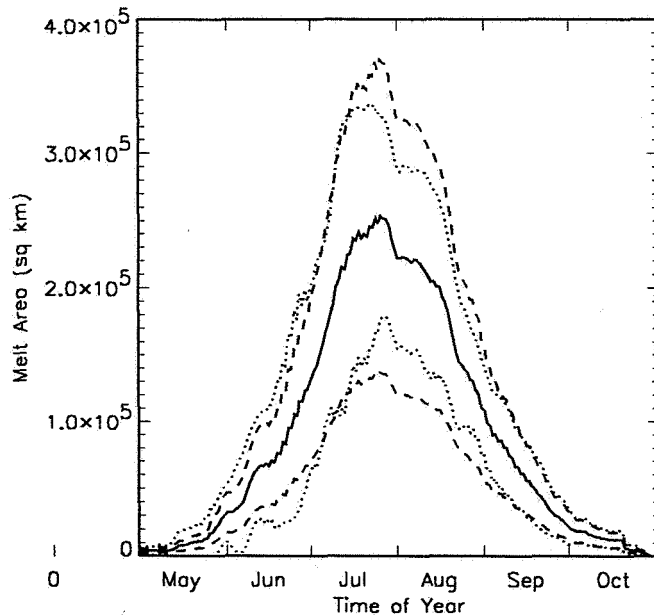*Figure 4.2*   The average spatial melt extent for the years 1979-1994 (solid line), mean melt ±1 standard deviation (dotted line), and melt area for 1°C temperature change (dashed line) in km² for the melt months of June, July and August. The extent was calculated by determining the mean area coverage for these months in each year and then averaging these values over the entire coverage period.
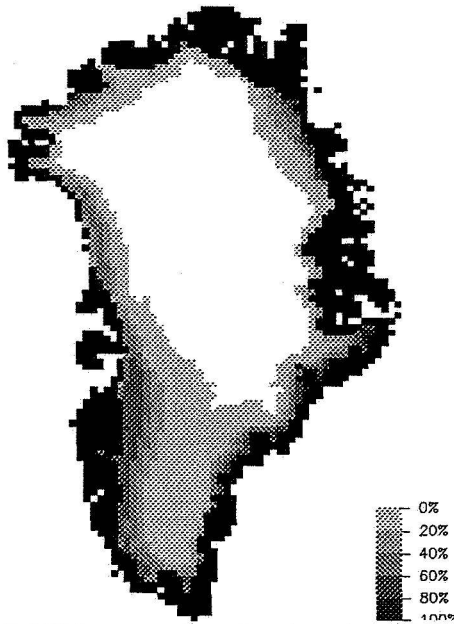
Figure 4.3   *1979-1994 composite of melt. Annual composites of melt. The shaded areas are areas that experience melt in the month shown at least once in the period from 1979-1994. The different shades of gray indicate the percentage of time throughout the coverage period, the pixels experienced melt for the month shown. The white areas represent the dry snow areas, and the black areas are the locations of pixels that are not fully covered by the ice sheet.*
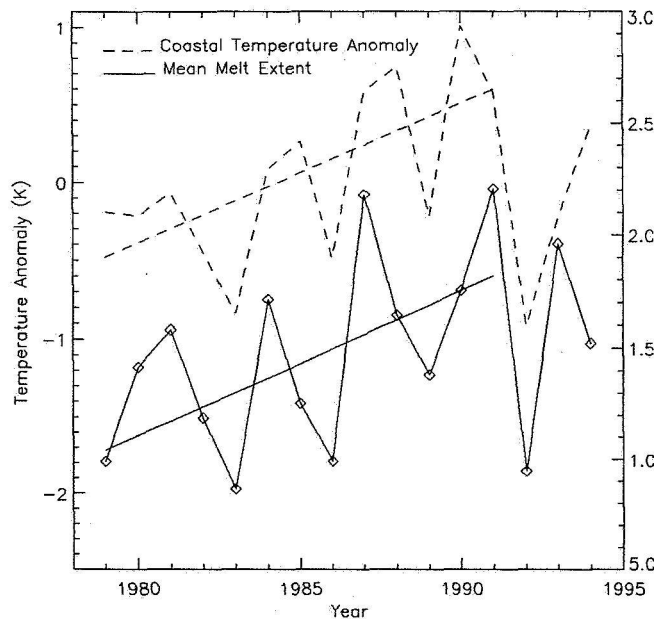
Figure 4.4   *Interannual variations in mean melt extent (average area for June, July, and August of each year) as determined by the XPGR classification technique for the years 1979-1994 (solid line). The years 1978-1991 show a 4.5% increase in areal melt extent, which is consistent with the increase observed by Mote and Anderson (1995), though slightly greater (Mote and Anderson reported a 3.8% increase). In 1992, following the eruption of Mt. Pinatubo, the melt area decreased considerably, before continuing to rise again in 1993 and 1994. Also shown (dashed line) are the coastal temperature anomalies from six coastal climate stations along Greenland's perimeter for the same period.*

5. 1 PASSIVE MICROWAVE ACCUMULATION RATES

5. 1 Introduction

A direct relationship between snow accumulation and microwave emissivity (e) in the dry snow regions of the Greenland and Antarctic ice sheets has been shown (Zwally, 1977, Comiso et al., 1982, Zwally and Giovinetto, 1995). This relationship is manifested in the microwave brightness temperature (Tb) according to the Rayleigh-Jeans approximation:

$$Tb = eTp$$

where Tp is the effective physical temperature of the emitting snow.

Significant changes in brightness temperature were observed during the SMMR coverage period in the dry snow regions of the ice sheet (Steffen et al., 1993). In some instances the average Tb increased by 18 K in six years with the strongest trends located in the northeast portion of the ice sheet (Fig. 5.1) where accumulation is lowest (Ohmura and Reeh, 1991). It has been theorized that these trends may be attributable to variations in accumulation rates and the associated changes in volume scattering, since they are so severe, and apparently not linked to temperature changes (Steffen et al., 1993).

The relationships are complicated by the summertime development of surface hoar which also impacts the microwave signal (Shuman et al., 1993). Using a DIScrete Ordinate Radiative Transfer model, DISORT (Stamnes et al., 1988), the relative effects of accumulation and hoar development on the microwave emission are examined. Also discussed are a method of improving accumulation estimates from ice cores, and a first-order hoar parametrization technique.

5.2 Method

5.2.1 Radiative Transfer Model

A 16 stream 20 layer DISORT model was constructed to represent the polar firn in the dry snow regions of the ice sheet. The microwave emission at 19.35 GHz vertical polarization was modeled for 53° angle and winter conditions at Inge-Lehman (77° 57' N, 39° 11' W; see Fig. 5.2). The model was a multiple scattering model based on those of Zwally (1977), and Comiso et al., (1982). Unlike those models, however, a layer was included to represent summertime hoar development.

After the model was run for Inge-Lehman, it was modified for different accumulation rates and temperatures (according to Gow's (1971) grain growth rate equation) to represent Summit conditions (72° 18' N, 37° 55' W; see Fig. 2). This was done so some initial comparisons could be made to a limited amount of in situ ice core data (Bolzan and Strobel, 1993). To make these comparisons, it was necessary to develop a proxy for the amount of hoar formation and to improve the ice core accumulation estimates.

5.2.2 Hoar Parameterization

Shuman and Alley (1993) showed that a sustained decrease of the SSM/I 37V/37H ratio in the summertime is often indicative of a hoar formation event. Such a sustained decrease is observed in most summers of the 1978-1995 coverage period, and were used to establish a proxy for the extent of hoar formation. Five day periods, or more, that show a sustained decrease in this ratio were identified, and the cumulative change in the ratio for each summer is calculated. By dividing the cumulative decrease in a given season by the mean annual decrease for the coverage period (1979-1994), an index for the amount of surface hoar formation is obtained. The index is then weighted and used to scale the brightness temperature, in order to account for the hoar effects.

The weight of this scaling parameter is determined by running the DISORT model for a typical case at Summit in which 1.5 cm of hoar forms during the summer (C.A. Shuman, personal communication). The percentage of contribution from this "average" hoar layer, as determined by the model, is used to scale the hoar index, and this scaled index is then applied to the observed brightness temperatures. In this way, the variability is accounted for in the appropriate proportion, and a brightness temperature more dependent on accumulation can be achieved.

5.2.3 Improved Ice Core-Based Accumulation Estimates

Ice cores have provided among the most commonly accepted estimates of snow accumulation for an area. These estimates are made by determining the mass of firn that lies between various peaks and troughs in oxygen-18 isotope concentrations (δO^{18}) which indicate annual layers (discussed in Bolzan and Strobel, 1994). A significant problem arises in that each winter isotopic trough is assumed to occur in December of the given year, and each summer peak is assumed to occur in June. These dates may be off by two months in either direction (J. Bolzan, personal communication), resulting in a significant uncertainty. This uncertainty can be reduced considerably by determining the date of minimum and maximum smoothed 37V brightness temperatures to identify the times of coldest and warmest temperatures.

5.3 Results

The emissivity dependence on accumulation and on hoar thickness for Inge Lehman is shown in Figure 5.3. The results indicate a number of significant relationships:

1.   Not only does the emissivity increase with increasing accumulation, but its sensitivity is greatest in the low accumulation areas. This occurs because in high accumulation areas, new snow already comprises a large part of the signal as compared to areas where the accumulation is low; thus changes are less likely to impact the overall signal. The relationship is consistent with the locations of the strongest trends in the areas of lowest accumulation.

2.   The sensitivity of emissivity to accumulation is greater with increasing hoar layer thickness. This is most likely because the high scattering characteristics and large optical thickness of the hoar layer result in significant extinction of the upwelling radiation from the snow below. As a result, in the presence of a thick hoar layer, more of the signal comes from the near surface layers of snow; thus the sensitivity is greater.

3.   Emissivity is largely dependent on the hoar layer thickness itself. Variations in hoar thickness of a few millimeters, have roughly the same impact on the emissivity as ten centimeters of accumulation changes.

4.   A hoar layer thickness of 1.5 cm, reduces the emissivity by 2.8 percent (approximately 5 K) when compared to an area without hoar. Therefore, in order to derive accumulation from observed brightness temperatures, the hoar must be considered. The differences in Tb for conditions with and without hoar considerations are shown in Figure 5.4.

5.   The average date of minimum temperature for the SMMR - SSM/I coverage period (1978-1994) is January 17, with a standard deviation of 31 days. This variability is significant and should be accounted for.

6.   The accumulation and hoar effects at Summit (Fig. 5.4) are outweighed by the temperature effects. For the nine years of overlapping accumulation and Tb data (1979-1987), accumulation is loosely correlated to brightness temperature (R=0.55). The hoar index appears to have the same magnitude of

correlation, but inversely so (R=-0.51). This inverse correlation is expected since extensive hoar development reduces the brightness temperature. After applying the hoar index to the brightness temperatures, however, the correlation disappears. The fact that the brightness temperature variations are only on the order of 5 K, which can conceivably be attributable to temperature variations, makes knowledge of the temperature conditions critical. Work is currently under way to determine these temperatures from Advanced Very High Resolution Radiometer (AVHRR) data, but they have not yet been determined (J. Stroeve, work in progress).

The analysis was limited to Summit because it is the only location for which ice core data on accumulation were available. Unfortunately, this is an area for which the observed Tb variability was not very strong. The observed trend near the proposed TUNU-North site of the Program for Arctic Regional Climate Assessment (PARCA) was approximately 18 K during the SMMR years, which exceeds any likely temperature effects. As a result, when core data are obtained from TUNU, and surface temperature estimates are made, the model can be validated and improved.

5.4 Conclusion

The radiative transfer model appears to accurately represent the emission behavior of snow under changing conditions of accumulation and hoar development. The link between microwave emission and accumulation rates in the dry snow area of the Greenland ice sheet is significant. However, the emissivity is even more dependent on the extent of hoar development. As a result, accumulation estimates based on passive microwave observations require successful parameterization of the hoar formation characteristics.

Until this hoar development can be adequately parameterized, the detection of interannual variations in accumulation will not be possible. The observed trends for the Inge Lehman region are most likely due primarily to changes in hoar development, and secondarily to changes in accumulation rates.

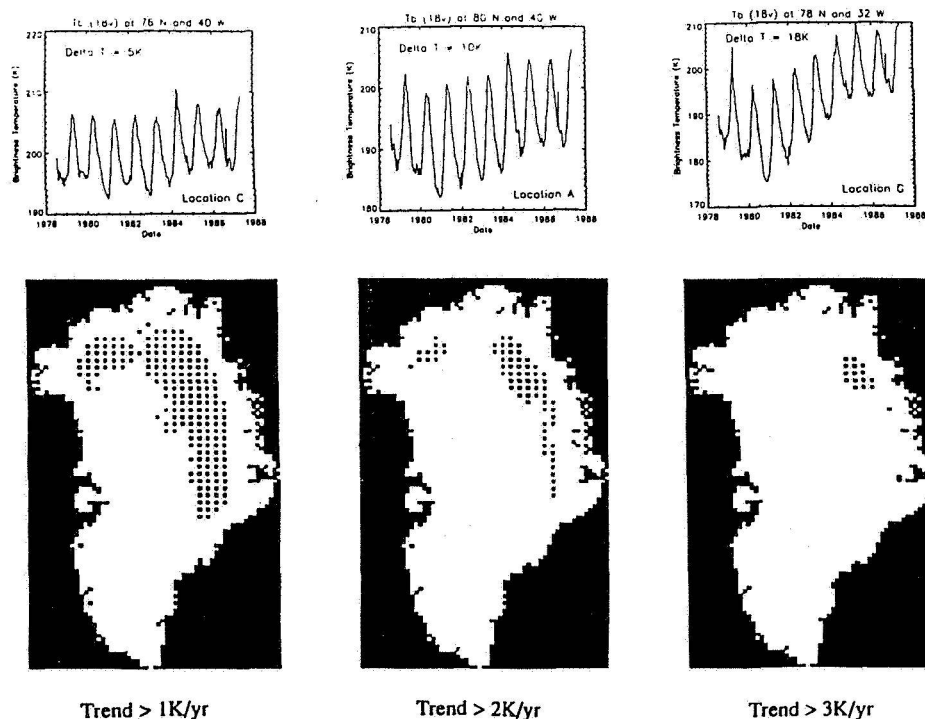Trend > 1K/yr   Trend > 2K/yr   Trend > 3K/yr

Figure 5.1   *Locations of 18V Tb trends of varying magnitude. The strongest trends are located in the northeast region of the ice sheet, which is the low accumulation zone.*

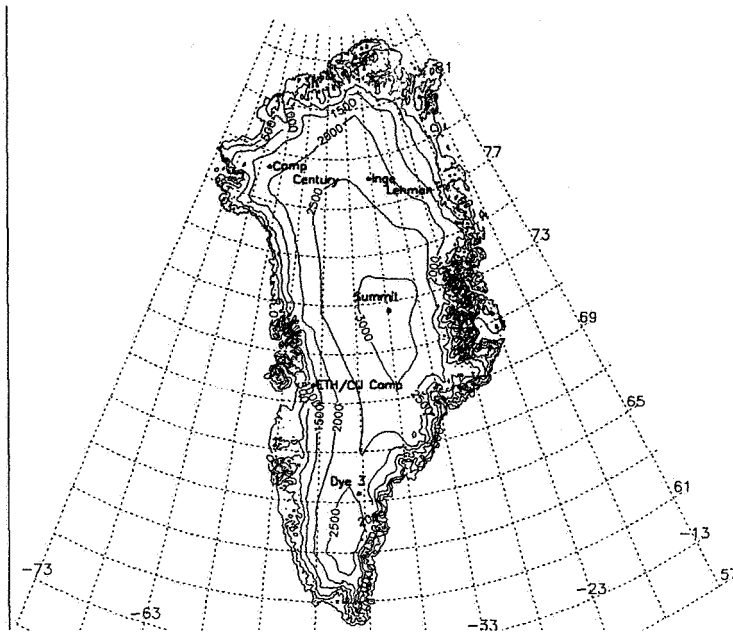*Figure 5.2.   Elevation map of the Greenland ice sheet. Inge-Lehman and Summit are the locations for which the model was run. These were chosen because of the availability of a limited amount of in situ data.*
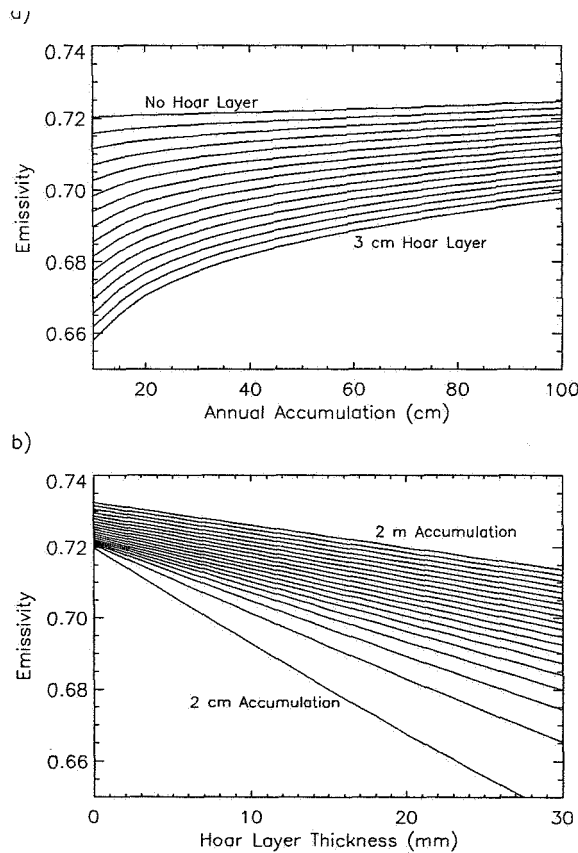
Figure 5.3   Dependence of microwave emissivity on accumulation and hoar thickness at Inge Lehman (77° 57'N, 39° 11'W). The sensitivity to hoar formation is much greater than to accumulation variations.
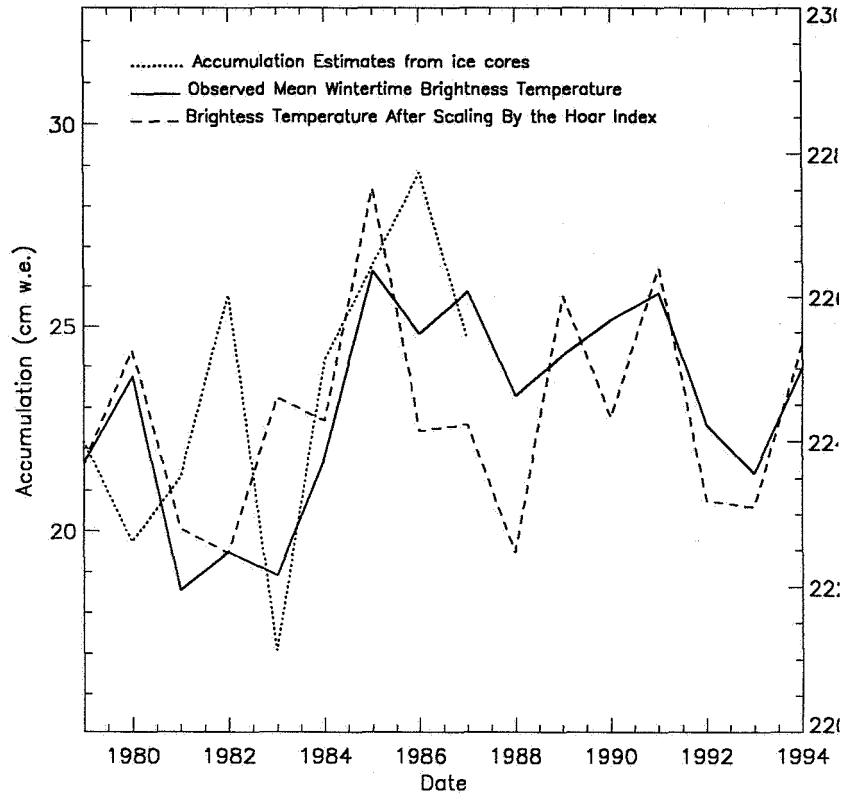
Figure 5.4   *19V brightness temperatures before and after adjusting for the hoar development. The presence or absence of hoar can change the Tb by several K. Also shown for comparison are the accumulation rates as derived from ice core analysis. Without including temperature effects, there is essentially no correlation between the accumulation and the brightness temperatures.*

6. ELEVATION CHANGES ZONE NEAR THE SWISS CAMP

6.1 Objectives

The scientific objective is to investigate seasonal and interannual changes of the ice surface elevation in the equilibrium zone. Additional objectives are: to define the capability of GPS for measuring vertical motion of the ice; to compare elevation changes obtained from GPS, airborne laser altimetry, and satellite radar altimetry; and to assess the utility of very high-resolution imagery for mapping ablation zone features and surface melting.

6.2 Method

Differential GPS measurements are made at pairs of poles separated by about 116 meters along the flowline, which is approximately the annual horizontal displacement. Measurements are repeated at annual intervals. Since the upstream pole moves to the position of the downstream pole of each pair in one year, the vertical ice velocity can be determined directly, and compared with the velocity calculated from measurements at one pole using the measured slope. Complementary measurements of the surface mass balance are made by the University of Colorado.

Pole pairs were placed at the Swiss Camp, which was established at the location of the equilibrium line in 1990 and at 2.3, 3.3, and 4.3 km downstream. The set of poles at the camp was measured in May of 1994 and 1995 and the downstream poles after emplacement in May 1995.

The Goddard/Wallops aircraft laser-altimeter mission over flew the flowline through the camp in 1994 and again in 1995.

6.3 Results

The horizontal velocity at the camp is 34.8 cm/day at an azimuth of 233 degrees (southwest), as obtained from GPS measurements over 6 days. Imagery was used for mapping of melt features and identification of crevasse fields in the area of the survey poles.
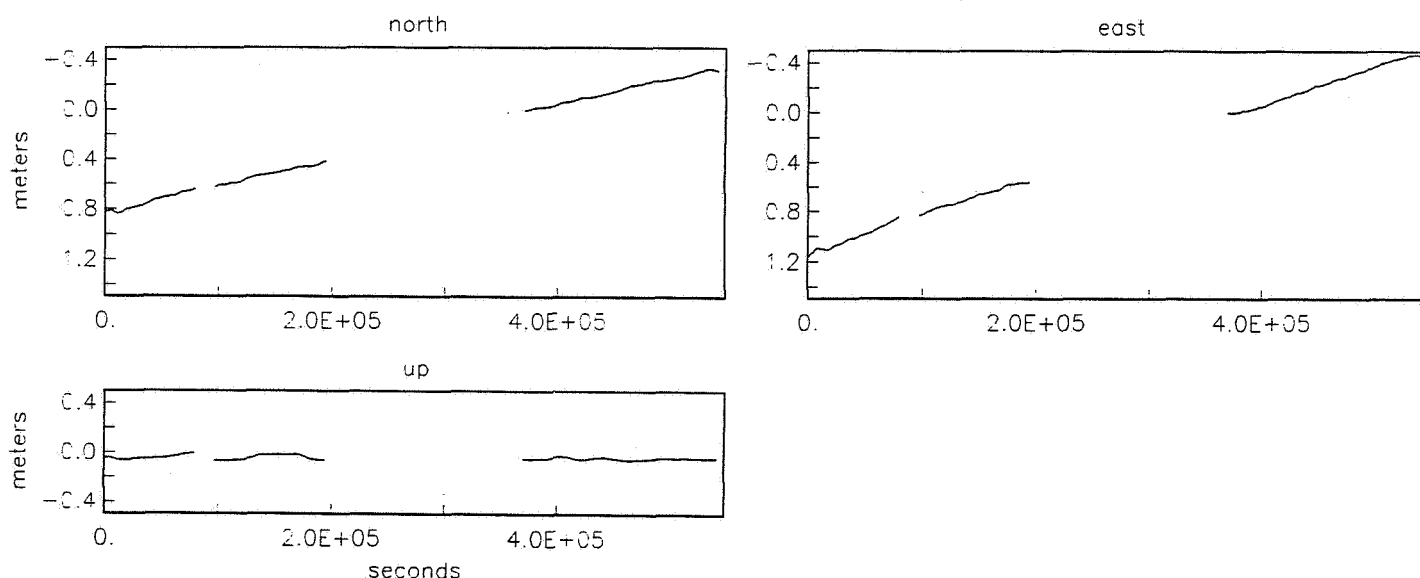

Figure 6.1   3-D motion at Swiss camp May 14 to May 20, 1995 from GPS (Analysis by Kristine Larson, U. of Colorado)

7. GEODETIC ICE INVESTIGATIONS

Dipl.-Ing. (FH) Jürgen Kreutter,
Prof. Dr.-Ing. Manfred Stober

7.1 The geodetic program 1995

In the period from May 27 to June 20 a geodetic program was performed by scientists from the "Hochschule für Technik Stuttgart". Dipl.-Ing. (FH) J. Kreutter was working at the ETH/CU-station and Prof. Dr.-Ing. M. Stober at the GPS reference point in Jakobshavn.

The measuring program was:
- Baseline Jakobshavn-Camp (about 80 km) by GPS with 9 sessions,
- Re-measurement of the deformation figure (triangle with central point, ranges about 1 km) by GPS and EDM,
- Reconstruction and re-measurement (GPS) of old positions from the year 1994,
- Topographical survey of the snow and ice surfaces around the camp.

7.2 Velocity of ice movement and height change

7.2.1 Fundamental Data

The GPS measurements were referred to the same point on solid rock like in 1990, 1991 and 1994 (JAKOBSHAVN, No. EUREF 0112). But for the first time as reference of calculations the newest coordinates in the EUREF system were used (for comparison of positions 1994 and 1995). The Camp Point 101 was attached at 5 days during the period from June 16 to June 19 with altogether 9 sessions at 3 hours measuring time each. Like in 1994 the GPS measurements were performed by GPS receivers LEICA System 200. All GPS results are now referred to the following WGS84-coordinates as shown in the Table 7.1.

Table 7.1 WGS84-coordiantes used for Jakobshavn (EURF 0112) and the ETH/CU Camp (Camp 101).

Point	WGS-X	WGS-Y	WGS-Z	Ellips. height
EUREF 0112	1424822.44	-1765538.53	5941079.97	72.307
Camp 101 (15.6.95)	1456107.072	-1693289.759	5955598.550	1175.922

7.2.2 Velocity of Ice Movement

The adjusted values of 5 observation days show a change in slope distance of -0.324 m/day (Fig. 7.1). Reduced to the flow direction, which is 8.61 gon different from the observed azimuth Jakobshavn-ETH/CU Camp, we obtain an actual flow velocity of 0.327 m/day. Looking to the residuals from the adjustment during the 9 sessions we have to consider errors of a single distance in a range up to one meter.
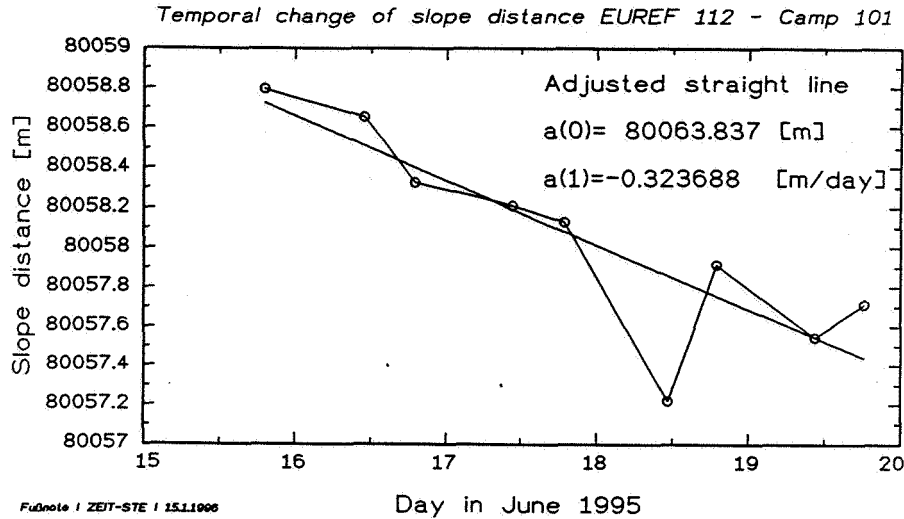
Figure 7.1   Temporal change of the slope distance Jakobshavn (EUREF 0112) - ETH/CU-Camp (101) from a
short observation period (9 sessions in 5 days).

The comparison between the positions of point 101 in 1994 and 1995 is not influenced by possible
seasonable changes. Here we obtain a slower horizontal flow velocity of 0.316 m/day. The difference may
result from another velocity during summer and winter periods, but that is not sure as long as the real
accuracy of short time GPS measurement is not examined in more detail. Such a study is planned for 1996.
We also have to consider local effects due to different topography, as we see from the 4 points in the
deformation net (Table 7.2, compare section 7.3, too).

Table 7.1   Flow velocity and flow direction in the period 1994-1995

point	displacement of point (m / day)	azimuth of movement (gon)
106.001	0.3233	260.5388
120.001	0.3261	260.0891
121.001	0.3204	259.5326
122.001	0.3265	260.1553
average	0.3241	260.0790

7.2.3 Flow Direction

It is not possible to determine the azimuth of flow direction from only 5 days of observation with an
satisfying accuracy. From the one year period between 1994 and 1995 we find α = 260.0790 gon (average
of 4 points in the deformation net). This value is only slightly different from the long periodic value from
1991 to 1994 (α = 260.6020 gon), which probably may be caused by local topographic influences.

7.2.4 Height Changes

The most important glaciological parameter is the temporal height change of the ice surface at the same position. For this purpose the old positions of 4 points have been reconstructed in the field by GPS. The measured heights at the snow surface were reduced to the actual ice horizon by snow pits, showing the stratigraphic layers (compare Table 7.3). The resulting actual change of ice heights 1994- 1995 are shown in the following Table 7.2.

Table 7.2   *Height change of the ice surface in the period from 1994 to 1995*

Point No.	Snow height (m) 1995	Ice surface change (m) 1995-94
106.001 (C)	0.60	-1.057
120.001 (A)	0.80	-0.472
121.001 (B)	0.64	-0.196
122.001 (D)	0.76	-0.432
average*	0.73	-0.375

* without 106.001

Bigger discrepancies against the average height change only occur at point 106, which is situated very close to the camp, so it might be falsified by influences like wind drift and artificial snow accumulation. Neglecting point 106 we obtain a yearly averaged height diminution 1994-1995 of -0.375 m. In the period from 1991 to 1994 we had found a height diminution of -0.20 m/year.

The difference against the longer periodic height change might be explained by the low accuracy of a single GPS positioning, as it was used in the previous campaign (1994). Analyzing the residuals from the averaged height during the 9 sessions in 1995 (5 days) we see, that the ellipsoidal height is varying in a range of about 1.5 m, although the height can be adopted as constant during this short period (Fig. 7.2). Neglecting the disturbed measurement of the first session on June 19, 1995, the standard deviation of one height determination is $s_0 = \pm 0.42$ m, that of the average is $s = \pm 0.15$ m. Although further investigations in the accuracy of GPS heights are very important, we can accept an averaged diminution of the ice height of - 0.24 m/year since 1991 as realistic and significant.
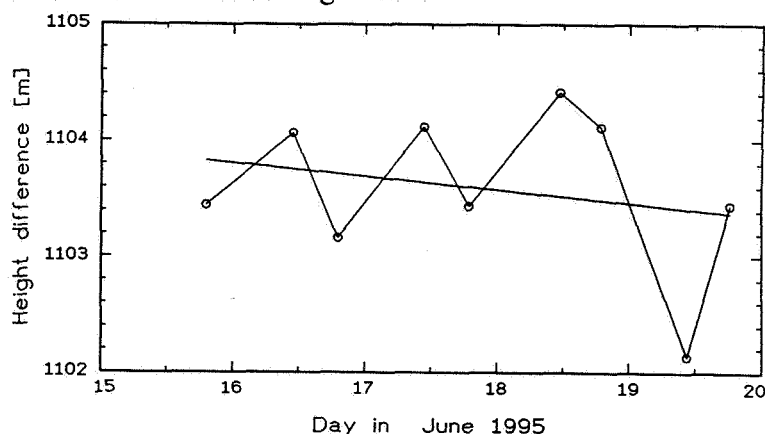

Figure 7.2   *Residuals from the adjusted ellipsoidal height difference Jakobshavn (EUREF 0112) - ETH/CU-Camp (101) from short periodical observations (9 Sessions in 5 days).*

7.3 Deformation

A first impression of the locally differing flow vectors had already been shown in Table 7.1. Consequently the deformation of the whole figure (triangle with a central point) is an in-homogeneous one. After transformation of the net from 1995 on that of 1994 there are remaining deviations from 0.24 m up to 1.52 m (Fig. 3). The recent distortions (DS/S) of the ranges (S) are summarized in Table 7.3, together with the old values for the period 1991-1994, such as mentioned in the Progress Report 1995. Generally, they are agreeing well in the signs, with small deviations in the amount.

Table 7.3   Distortions 1994 - 1995 and comparison to 1991-94

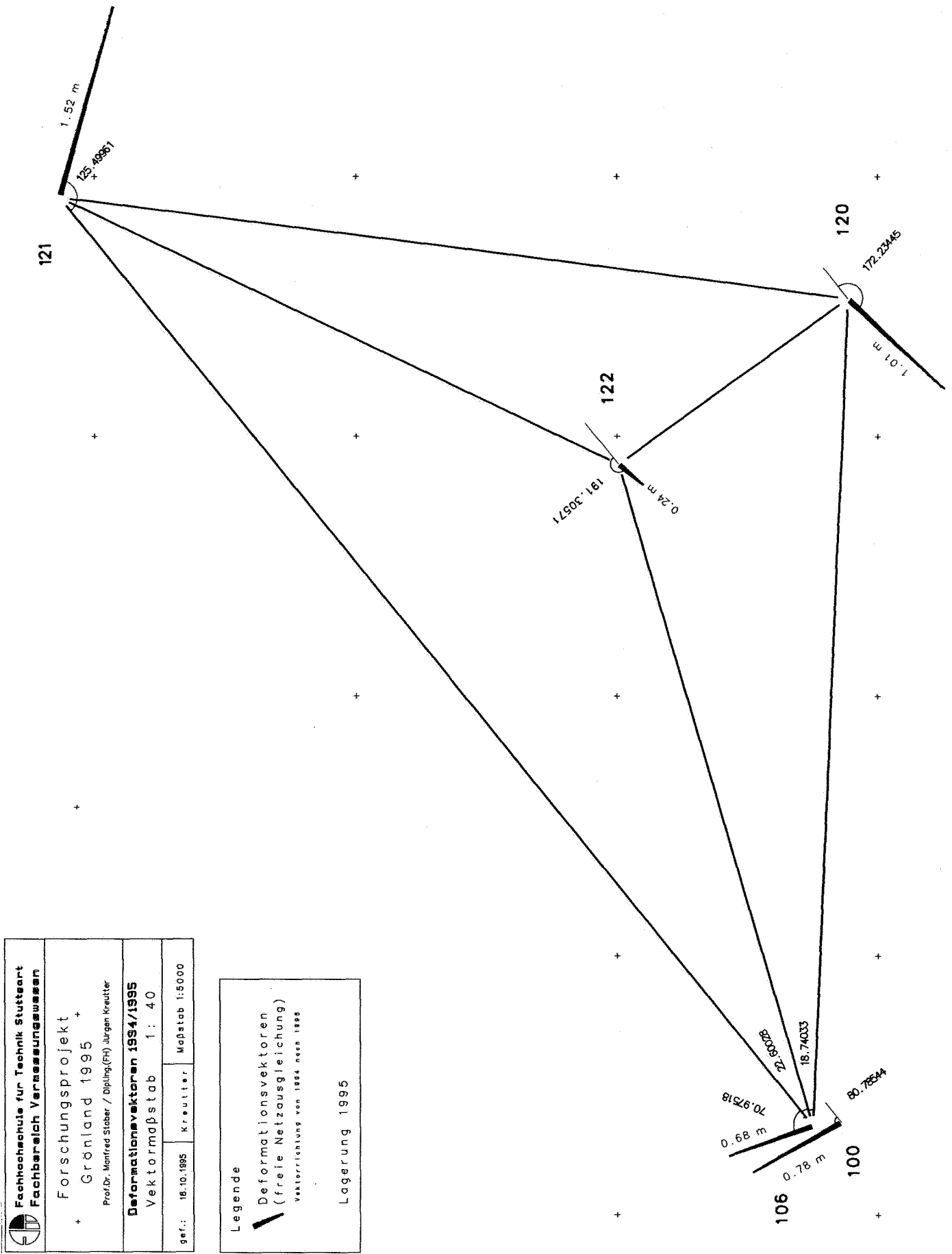| point name new, (old)	spatial length (m) 1995	1994	DS (m) 94-95	DS/S ppm 91-94	DS/S per day	DS/S per day
106(C) - 122(D)	663.414	663.565	-0.151	-228	-0.62	-0.03
106(C) - 121(B)	1149.619	1148.961	+0.658	+573	+1.57	+1.79
121(B) - 120(A)	762.200	761.603	+0.597	+784	+2.15	+1.72
122(D) - 120(A)	272.527	272.396	+0.131	+480	+1.32	+2.08
106(C) - 120(A)	797.600	797.991	-0.391	+490	-1.34	-0.19
121(B) - 122(D)	594.362	593.867	+0.495	+834	+2.28	+2.04

7.4 Topography

A topographical survey with many points around the camp area was performed by a single GPS receiver (rover) in relation to the GPS-reference point 101. As measuring procedure the "stop-and-go" method was used with measuring time of only few seconds at each point, for which usually we can expect an accuracy of centimeter. But the adjusted terrain model (calculated by the program SCOP) shows an accuracy of only 0.25 m, and 4.1% of all the points have been detected as wrong despite of indicating a correct ambiguity solutions. So we see again the lower accuracy of GPS heights under the special conditions on the Greenland ice sheet.

Nevertheless the adjusted topographical map is showing a good impression of the snow surface (Fig. 7.4) around the camp area. In the vicinity of the camp, the snow surface is considerably disturbed by wind drift, as is shown in the perspective view in the grid model (Fig. 7.5). In addition to the GPS positioning at each terrain point the depth of the snow layer was measured to produce a topographical map of the ice surface and isolines of the snow (Fig. 7.6).

We also produced inclination models from snow and ice surfaces, which are not presented here. For detailed studies concerning the terrain inclination we show two cross-sections in North-South (Fig. 7.7) and West-East direction (Fig. 7.8) respectively. Further, we found the beginning of a crevassed area approximately 2.5 away from the camp, in direction South-West (Fig. 7.9). The azimuth 235° is almost the same one as the flow direction, so the camp would reach this area in about 19 years.

Figure 7.3   Deformation analysis of networks 1994-1995

Figure 7.4   Topographical map of snow surface in June 1995 around the area of the ETH/CU-Camp.

Figure 7.5   *Grid model of the snow surface around the ETH/CU-Camp in June 1995*


```
XO =        -32.35     Maschen=1.0 m
YO =        -46.95     Gittermaßst Z = 3
ZO =       1148.86
```
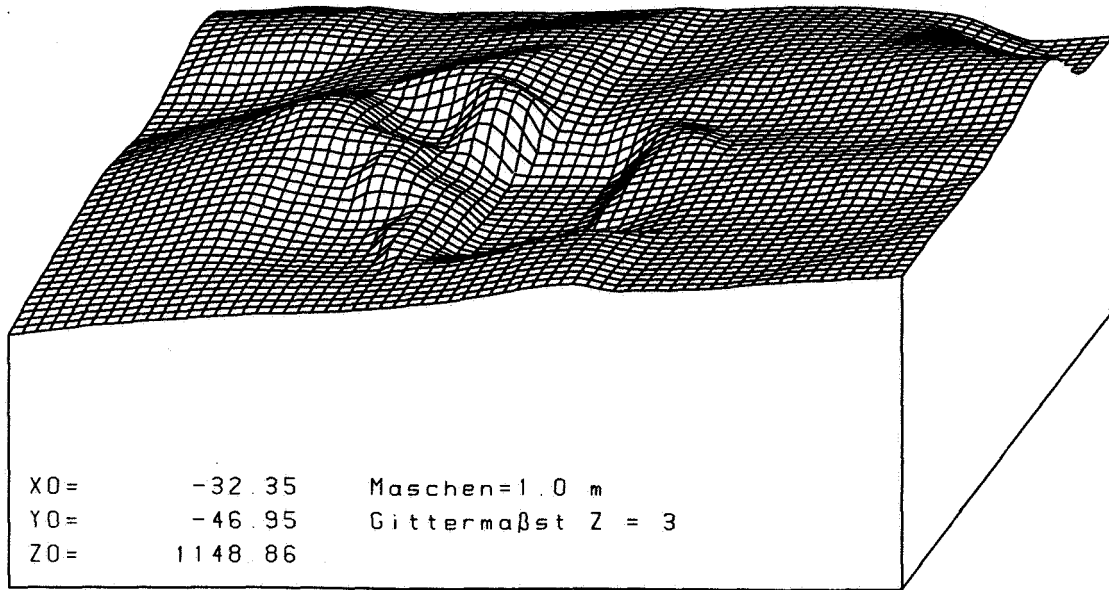
Fachhochschule für Technik Stuttgart
Fachbereich Vermessungswesen

Forschungsprojekt
Grönland 1995

Prof.Dr. Manfred Stober / Dipl.Ing.(FH) Jürgen Kreutter

Gittermodell Campumgebung

| gef.: 18.10.1995 | Kreutter | Maßstab |

Figure 7.6   *Isolines of snow thickness around the ETH/CU-Camp in June 1995.*
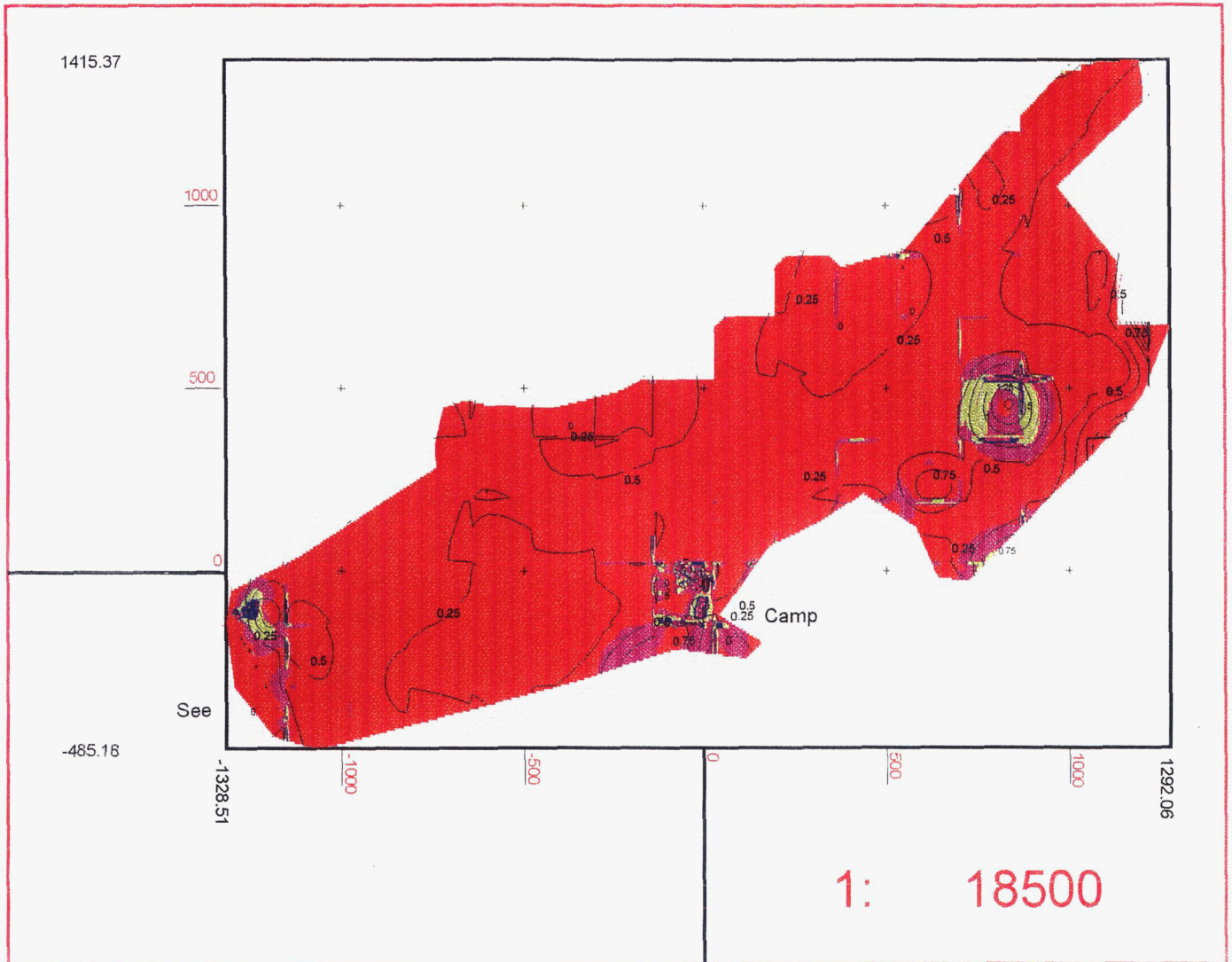
Groenland 1995

Differenzmodell

**Differenz zwischen
Schneeoberfläche und Eisoberfläche**

1.) Isolinien

2.) Neigungsmodell
über Farbflächenzuweisung

Legende

Farbe	Neigungsbereich
■	0.5 % Neigung
▨	1.0 % Neigung
▨	1.5 % Neigung
■	2.0 % Neigung

Figure 7.7 Cross-section of snow thickness heights in North-South direction (ETH/CU-Camp, June 1995).

Figure 7.8   *Cross-section of snow thickness heights in West-East direction (ETH/CU-Camp, June 1995).*

Forschungsprojekt Grönland 1995
Dipl.-Ing (FH) Jürgen Kreuter
Fachbereich Vermessungswesen

FACHHOCHSCHULE HOCHSCHULE FÜR
STUTTGART TECHNIK

Längsprofil
Campumgebung

Ost - West Richtung

Höhenangaben im lokalen Höhensystem 1995

WGS 84 Höhen :
lokale Höhen + 1075.21 m

Lageskizze

Profil 1
Ost - West Richtung

Camp
Holzplattform

STATION	HOEHE
072.00	100.31
070.00	100.27
068.00	100.23
066.00	100.19
064.00	100.11
062.00	099.98
060.00	099.78
058.00	099.52
056.00	099.21
054.00	098.90
053.64	098.85
052.00	098.85
050.00	098.85
048.00	098.85
046.03	098.85
046.00	098.86
044.00	099.21
042.00	099.62
040.00	100.15
038.00	100.64
036.00	100.95
034.00	101.10
032.00	101.12
030.00	101.03
028.00	100.89
026.00	100.75
024.00	100.60
022.00	100.43
020.00	100.26
018.00	100.09
016.00	099.95
014.00	099.82
012.00	099.68
010.00	099.58
008.00	099.53
006.00	099.47
004.00	099.40
002.00	099.32
000.00	099.23

97.00

HOEHE
STATION
LAENGSPROFIL

MASSSTAB DER LAENGEN: 1 : 312,5
MASSSTAB DER HOEHEN: 1 : 125

Groenland 1995

Figure 7.9   *Topographical map of a crevasse at a distance of 2000 m from ETH/CU camp. The maximum crevasse depths was 25 m, with a width of 2 m. The GPS measurement was taken in June 1995.*

Gletscherspalte

Ab hier in südlicher Richtung sind mehrere

Gletscherspalten aus der Luft erkennbar.

From: 101
To: 9500
Azi: 234 56 48.990
Hdist: 2201.078 m
Hdiff: -8.544 m

1000 m
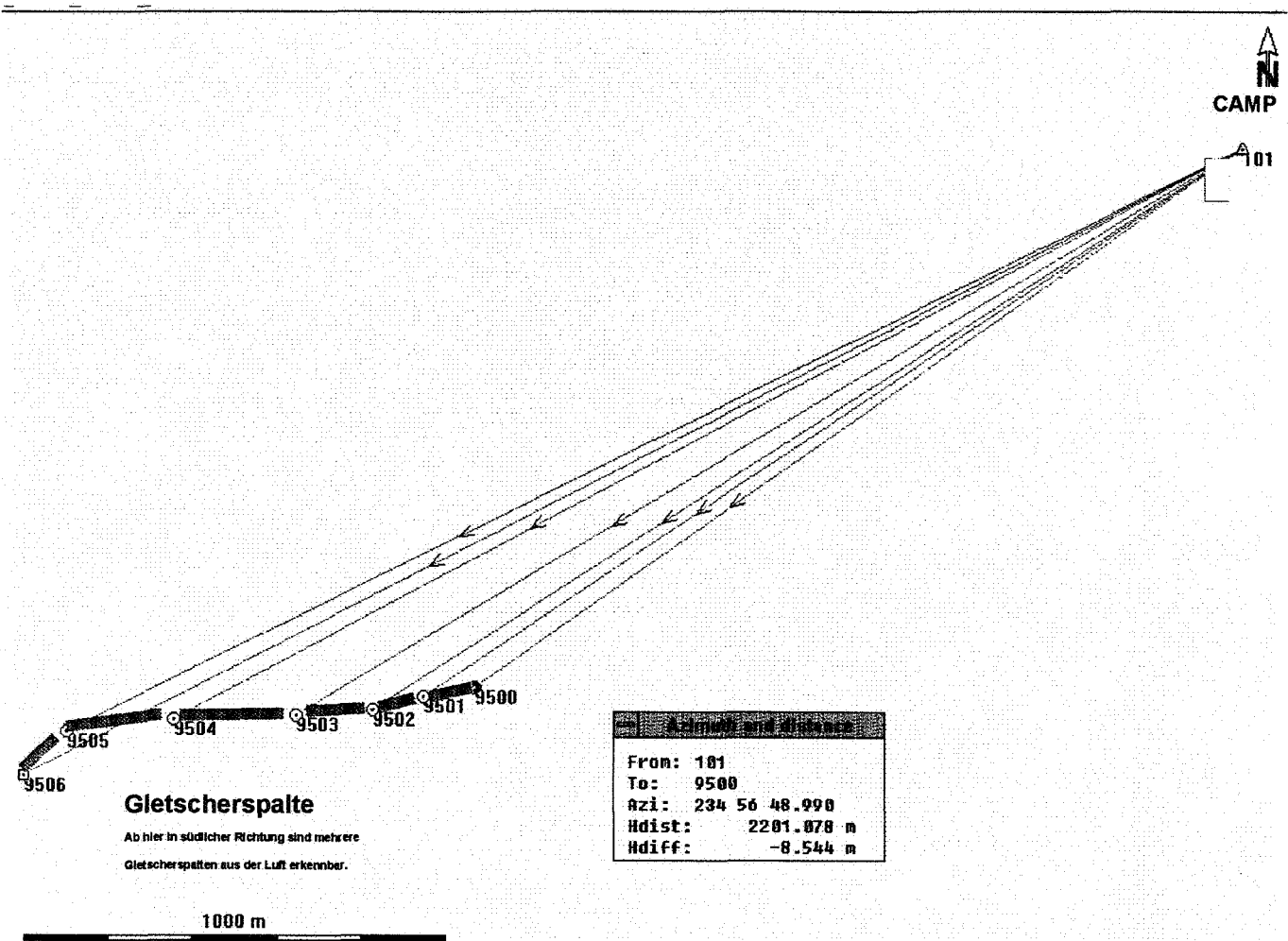
REFERENCES

Abdalati, W., and K. Steffen 1995, Passive microwave-derived snow melt regions on the Greenland Ice sheet. Geophys. Res. Let., 22, 787-790.

Binenko, V.I. and H. Harshvardhan, 1993, Aerosol effect in radiation transfer, In: Aerosol Effects on Climate, The University of Arizona Press, pp. 190-227.

Comiso, J. C., H. J. Zwally, and J. L. Saba, 1982, Radiative transfer modeling of microwave emission and dependence on firn properties, Annals of Glaciol., 3, 54-58.

De Abreu, J. Key, J.A. Maslanik, M.C. Serreze, and E.F. Le Drew, 1994, Comparision of in situ and AVHRR-derived broadband albedo over arctic sea ice, Arctic, 288-305.

Dozier, J., and S.G. Warren, 1982, Effect of viewing angle on the infrared brightness temperature of snow, Water Resources Res., 18, 1424-1434.

Groisman, P.Ya., K.R. Thomas, and R.W. Knight, 1994, Changes of snow cover, temperature, and radiative heat balance over the northern hemisphere, J. Climate, 7, 1633-1656.

Haefliger, M., K. Steffen, and C. Fowler, 1993, AVHRR surface temperature and narrow-band albedo comparison with ground measurements for the Greenland ice sheet, Annals of Glaciolology, 17, 49-54.

Hillamo, R.E., V.M. Kerminen, W. Maenhaut, F.L. Jaffrezo, S. Balachandran, C.I. Davidson, 1993, Size distribution of atmospheric trace elements at Dye 3, Greenland - I. Distribution characteristics and dry deposition velocities, Atmospheric Environment, 27A, 2787-2802.

Jaffrezo J.L. and C.I. Davidson, 1992, Sulfate in the air, surface snow, and snowpits at Dye 3, Greenland. In precipitation Scavenging and Atmosphere - Surface Exchange, Volume 3 (edited by Schwartz S.E. and Slinn W.G.N.) pp. 1693-1704. Proceedings of the fifth International Conference on Precipitation Scavenging and Atmosphere - Surface Exchange Processes, Richland, WA, 15-19, July 1992. Hemisphere, Washington D.C.

Jaffrezo, J.L., C.I. Davidson, and J.E. Dibb, 1993, Major ions in aerosols and surfacesnow during the Dye 3 Gas and Aerosol Sampling Program, Atmospheric Environment, 27, 2703-2727.

Key, J., and R.G. Barry, 1989, Cloud cover analysis with arctic AVHRR data 1. Cloud Detection, Journal of Geophysical Research, 94, 18521-18535.

Key, J. and M. Haefliger, 1992, Arctic ice surface temperature retrieval from AVHRR thermal channels, Journal of Geophysical Research, 97, 5885-5893.

Key, J., R. Stone, and M. Rehder, 1994, Estimating high latitude radiative fluxes from satellite data: problems and successes, IGARSS `94, Pasadena, 8-12 Aug. 1994.

Key, J., 1995, Streamer User's Guide. University of Colorado, 66 pp. (unpublished, 1994, 1995).

Li, Zhanqing and H.G. Leighton, 1992, Narrowband to broadband conversion with spatially autocorrelated reflectance measurements, Journal of Applied Meteorology, 31, 421-435.

Lindsay,R.W. and D.A. Rothrock 1994, Arctic sea ice surface temperature from AVHRR, American Meteorological Society, 7, 174-183.

McClain, E.P., W.G. Picher, and C.C. Walton, 1985, Compariative performance of AVHRR-based multichannel sea surface temperatures, Journal of Geophysical Research, 90, 11587-11601.

McMillin, L.M., 1975, Estimation of sea surface temperatures from two infrared window measurements with different absorption, Journal of Geophysical Research, 80, 5113-5117.

Miller, D.H., 1956, The influence of snow cover on local climate in Greenland, Journal of Meteorology, 13, 112-120.

Minnus, P., E. F. Harrison, L. L. Stowe, G.G. Gibson, F.M. Denn, D.R. Doelling, and W.L. Smith jr., 1993, Radiative climate forcing by the mount Pinatubo eruption. Science, 259, 1411-1415.

Mote, T.L., and M.R. Anderson, 1995, Variations in snowpack melt on the Greenland ice sheet based on passive microwave-measurements. J. Glaciol. 41, 51-60.

Ohmura, A. and N. Reeh, 1991, New precipitation and accumulation maps for Greenland, J. of Glaciol. 37(25), 140-148.

Price, J.C., 1983, Estimating surface temperature from satellite thermal infrared data - A simple formulation for the atmospheric effect. Remote Sensing Environment, 13, 353-361.

Rao, C.R.N., and J. Chen, 1995, Inter-satellite calibration linkages for the visible and near-infrared channels of the Advanced Very High Resolution Radiometer on the NOAA-7, -9, and -11 spacecraft, International Journal of Remote Sensing, 16, 1931-1942.

Salisbury, J.W., D.M. D'Aria, A. Wald, 1994, Measurements of thermal infrared spectral reflectance of frost, snow, and ice, Journal Geophysical Research, 99, 24,235-24,240.

Saunders, R.W. and K.T. Kriebel, 1988, An improved method for detecting clear sky and cloudy radiances from AVHRR data, International Journal of Remote Sensing, 9, 123-150.

Shuman, C.A., and R.G. Alley 1993, Spatial and temporal characterization of hoar formation in central Greenland using SSM/I brightness temperatures. Geophys. Res. Let. 20(23), 2643-2646.

Shuman, C.A., R.B. Alley, and S. Anandrakrishnan, 1993, Characterization of a hoar-development episode using SSM/I brightness temperatures in the vicinicty of the GISP2 site, Greenland, Ann. Glaciol., 17, 183-188.

Stamnes, K., S.Tsay, W. Wiscombe, and K. Jayaweera, 1988, Numerically stable algorithm for discrete-ordinate-method radiative transfer in multiple scattering and emitting layered media, App. Opt., 27, 2502-2509.

Steffen, K., Bidirectional reflectance of snow at 500-600 nm, Proceedings of the Vancouver Symposium, pp. 415-425, August 1987.

Steffen, K., W. Abdalati, and J. Stroeve, 1993, Climate sensitivity studies of the Greenland ice sheet using satellite AVHRR, SMMR, SSM/I, and in situ data, Meteorol. and Atmos. Phys., 51, 239-258.

Steffen, K., 1996. Spectral hemispheric and directional reflectance of snow, Journal of Geophysical Research, in press.

Stroeve, J., M. Haefliger, and K. Steffen, 1996:, Surface tempearture from ERS-1 ATSR infra-red thermal satellite data in polar regions, Journal of Applied Meteorology, in press.

Tanre, D., B.N. Holben, Y.J. Kaufman, 1992, Atmospheric correction algorithm for NOAA-AVHRR Products: Theory and Application, IEEE Transactions on Geoscience and Remote Sensing, 30, 231-250.

Van der Veen, C.J., and K.C. Jezek, 1993, Seasonal variations in brightness temperature for central Antarctica. Ann. Glaciol., 17, 303-306.

Wald, A., 1994, Modeling thermal infrared (2-14 mm) reflectance spectra of frost and snow, Journal Geophysical Research, 99, 24,241-24-250.

Warren, S.G. and W.J. Wiscombe 1980 A model for the spectral albedo of snow.I: pure snow, Journal of Atmospheric Science, 37, 2712-2727.

Wydick, J.E., P.A. Davis and A. Gruber, 1987, Estimation of Broadband Planetary Albedo from Operational Narrowband Satellite Measurements, NOAA Technical Report NESDIS 27, April 1987.

Zwally, H. J., 1977, Microwave emissivity and accumulation rate of polar firn, J. of Glaciol., 18(79), 195-215.

Zwally, H. J., A. C. Brenner, J. A. Major, R. A. Bindschadler, and J. G. Marsh, 1989, Growth of the Greenland ice sheet: measurement, Science, 246, 1587-1589.

Zwally, H. J., and M.B. Giovinetto, 1995, Accumulation in Antarctica and Greenland derived from passive-microwave data: a comparison with contoured compilations, Annals. of Glaciol., 21, 123-130.